

# Design of a Deep Sea LiDAR System

Laser Pulse Reception and LiDAR Control Logic

# Design of a Deep Sea LiDAR system

Laser Pulse Reception and LiDAR Control Logic

## BSc Thesis

Authors:	A.E. Admiraal	4545532
	B.M. Verdoes	4563263
Project duration:	February 11 - July 5, 2019	
Supervisor:	Prof. Dr. Ir. G.J.T. Leus	
Thesis committee:	Prof. Dr. Ir. G.J.T. Leus	
	Prof. Dr. Ir. K.L.M. Bertels	
	Dr. F. Uysal	
	Ing. F. van der Zwan	
	Dr. D. Elkouss Coronas	

With contributions from the entire electrical engineering work group of the SLiDAR team in chapters 2.  
*Bsc. Electrical Engineering 2019 BAP group A :*

A.E. Admiraal	4545532
J. Jonk	4577221
B. Minderman	4577868
B.M. Verdoes	4563263
L.R. Wix	4534654
E.P.M. Zwetsloot	4583817

This work builds on ideas from the mechanical engineering work group of the SLiDAR team.  
*Bsc. Mechanical Engineering 2019 BEP group A2 :*

D. Looman  
S.H.R. Rutten  
B.R. van Vliet  
D.O Wijnberg

In partial fulfilment of the requirements for the degree of

**Bachelor of Science**  
in Electrical Engineering

at the Delft University of Technology.

An electronic copy of this thesis is available at <https://repository.tudelft.nl/>.



# Abstract

Current subsea LiDAR implementations are inherently depth limited, and make LiDAR applications in the deep-sea costly. To this end, the SLiDAR project aims to develop a pressure tolerant LiDAR system for use at any ocean depth. This thesis elaborates the high-level system design of the LiDAR system, as well as the design and implementation of the laser pulse reception stage and the onboard central control unit. Due to the short time frame of the project and the high work load, the LiDAR system as a whole and its subsystems are not tested in practise. Hence, this thesis aims to provide a basis for future development, testing and verification of both the LiDAR system, its laser reception stage, and its central control unit.

# Preface

The Subsea LiDAR (SLiDAR) is a multidisciplinary Bachelor Graduation Project. The project team consists of 6 Bachelor of Electrical Engineering students and 4 Bachelor of Mechanical Engineering students. The idea for the project stems from the need of a ranging sensor on the Life OBserving Sea Traversing Explorer Robot (LOBSTER). The initial goal was to design a 3D laser scanning device based on the LiDAR principle that could work in the deep sea environment. As of writing this thesis, the design is left partially unfinished due to the large work load.

This thesis is one of a series of three theses on the electrical system design of the SLiDAR project. Each thesis is written by a subgroup of two project members, who implemented a specific subsystem of the LiDAR. Every thesis starts of with an almost identical chapter on the system design of the LiDAR. After that follows a chapter on the design of the subgroup specific subsystem.

We would like to thank Prof. Dr. Ir. G.J.T. Leus for supervising the project. Furthermore we would like to thank the MacArtney Group for letting us use their facilities for a reduced price. Finally, we would like to thank all members of the SLiDAR team for their efforts and enjoyable collaboration.

*A.E. Admiraal & B.M. Verdoes*

*Delft, June 2019*

# Contents

<b>1</b>	<b>Introduction</b>	<b>1</b>
<b>2</b>	<b>SLiDAR System Design</b>	<b>2</b>
2.1	Current underwater ranging methods . . . . .	2
2.2	A simple LiDAR system . . . . .	4
2.3	Functions of LiDAR systems . . . . .	4
2.4	Requirements. . . . .	5
2.5	Design options . . . . .	8
2.6	Concept selection . . . . .	12
2.7	Subsystem selection . . . . .	13
2.8	System modelling. . . . .	14
2.9	Functional Overview . . . . .	16
<b>3</b>	<b>The receiver stage</b>	<b>18</b>
3.1	Systems engineering . . . . .	18
3.2	Implementation . . . . .	20
3.3	TDC selection. . . . .	21
<b>4</b>	<b>Central Control Unit (CCU)</b>	<b>24</b>
4.1	Introduction . . . . .	24
4.2	Requirements. . . . .	24
4.3	CCU Design . . . . .	25
4.4	Testing and Validation . . . . .	29
4.5	Future Work. . . . .	29
<b>5</b>	<b>Conclusion</b>	<b>31</b>
<b>A</b>	<b>The polygon</b>	<b>36</b>
<b>B</b>	<b>Range Estimation Matlab Code</b>	<b>38</b>

## List of Abbreviations

### Acronyms

<b>ADC</b> Analog to Digital Converter	<b>PMT</b> Photomultipliers Tube
<b>APD</b> Avalanche photodiode	<b>RADAR</b> Radio Detection And Ranging
<b>CFAR</b> Constant False Alarm Rate	<b>RDT</b> Requirements Discovery Tree
<b>DOT</b> Design Option Tree	<b>ROV</b> Remotely Operated Vehicle
<b>FBS</b> Functional Breakdown Structure	<b>SfM</b> Structure from Motion
<b>FOV</b> Field Of View	<b>SLAM</b> Simultaneous Localisation And Mapping
<b>IC</b> Integrated Circuit	<b>SLiDAR</b> Subsea LiDAR
<b>LLS</b> Laser Line Scanning	<b>SNR</b> Signal to Noise Ratio
<b>LOBSTER</b> Life Observing Sea Traversing Explorer Robot	<b>SONAR</b> Sound Navigation And Ranging
<b>MEMS</b> MicroElectroMechanical Systems	<b>SPAD</b> Single-Photon Avalanche Diode
<b>OPA</b> Optical Phased Array	<b>SPI</b> Serial Peripheral Interface
	<b>ToF</b> Time of Flight
	<b>VCSEL</b> Vertical Cavity Surface Emitting Laser

# Introduction

Although deep water ecosystems are crucially important for human interests, they remain far from being fully understood [62]. It is simply very hard to get there. One of the challenges of subsea exploration is navigation. Satellite navigation signals are quickly attenuated in seawater and acoustic beacons are costly to set up. Conventional robotic systems employ Simultaneous Localisation And Mapping (SLAM) techniques to find their position from ranging information in this absence of positional references [49]. Limitations of subsea perception sensors make this difficult in the subsea environment [20].

LiDAR systems are often used in ranging applications above sea, but are not traditionally considered for use in subsea SLAM implementations [20]. Although subsea LiDAR systems exist, it is only marketed at asset inspection and metrology. Although it has high resolution and accuracy, the maximum scan speed of  $2 \text{ min}^{-1}$  [15] and high price of €500k probably contribute to its lack of application in subsea SLAM.

The goal of the Subsea LiDAR (SLiDAR) project is to explore the feasibility of an inexpensive subsea LiDAR system optimised for SLAM. This challenge is jointly tackled by a team of four mechanical engineering students investigating mechanical problems in their bachelor thesis and a team of six electrical engineering investigating electrical aspects in their thesis.

This thesis focuses on the electrical design, which is divided over:

- the transmission stage, generating high power laser pulses;
- the receiver stage, converting the Time of Flight (ToF) of the laser pulse to a digital reading;
- a scanning stage, distributing the distance measurements in space;
- a digital system, to time the measurements and communicate them to the outside world.

The present work motivates this division in part 2 and then details the design of the receiver stage and digital in parts 3 and 4 respectively. Figure 1.1 gives an overview of the system and illustrates the scope of these parts.

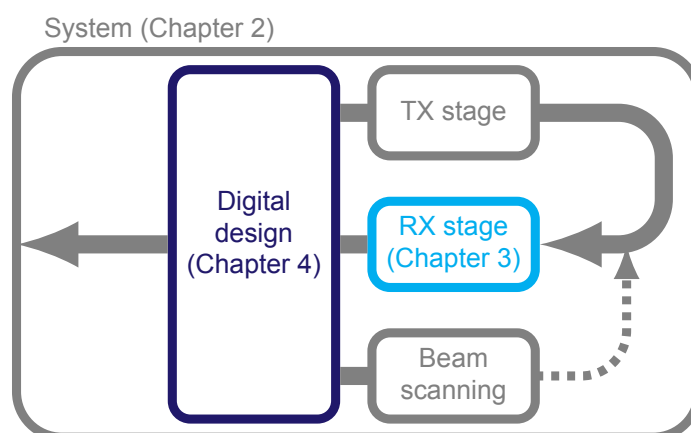


Figure 1.1: System overview.

## SLiDAR System Design

In this chapter, we explore system architectures suitable for SLAM capable deep sea LiDAR and establish a subsystem division for our implementation along with requirements on each subsystem. To this end, section 2.1 first motivates the choice to investigate deep sea LiDAR as a solution to the underwater SLAM problem by exploring its relation to current underwater ranging methods in a review of current underwater ranging methods. From there, section 2.2 will examine the system architecture of a simple LiDAR system for context, before we take the discussion to a more abstract point in section 2.3, identifying the fundamental functions of LiDAR systems. Section 2.3.3 will provide a summary of them in the form of a Functional Breakdown Structure (FBS) for a more visual overview. It will also serve as the basis of a Requirements Discovery Tree (RDT) in section 2.4.1, ensuring exhaustive coverage by requirements. Section 2.4.2 will detail them in a programme of requirements. Having established the functions of and requirements on the deep sea LiDAR, we will seek design options to fulfil these by analysing the state of the art of LiDAR techniques in section 2.5. These will be summarised in a Design Option Tree (DOT) in section 2.5.5, again providing a visual overview for further reflection. This reflection comes in the form of the selection of techniques best suited to our application to form a concept design by weighing their advantages and disadvantages in section 2.6. From here, functionalities are grouped in subsystems in section 2.7. This split generates the need for more detailed requirements on system-level key parameters. To find these, some system-level modelling is performed in section 2.8. Finally, section 2.9 gives a high-level overview of the proposed LiDAR design, and specifies the data flow on the interfaces between the made subsystems.

### 2.1. Current underwater ranging methods

This section explores the ways in which an underwater SLAM capable LiDAR could contribute to underwater SLAM by evaluating the strengths and weaknesses of current underwater ranging methods and investigating the unique role a LiDAR system could play.

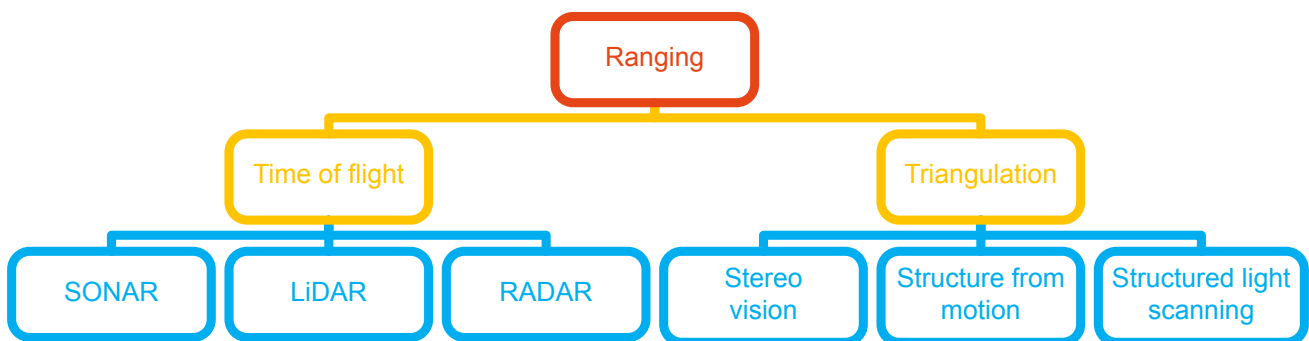


Figure 2.1: Classes of ranging methods. Adapted from [32, 24].

Current ranging methods can be classified as shown in figure 2.1. We distinguish two major classes based on the measured quantity:

- Triangulation methods estimate the distance to an object from the angles of at least two rays intersecting a certain point on an object.

- ToF methods estimate the distance to an object from the return time of an echo in a certain domain.

Triangulation methods can be further divided based on the types of angular measurements. A distinction can be made between stereo vision, structure from motion and structured light scanning. In industry, all of these systems are implemented optically. This introduces a trade-off between sensor size, sensitivity and resolution. Since sunlight does not reach the deep sea, there is also a trade-off between the sensor to illumination separation distance and interference due to volumetric backscatter.

Stereo vision uses concurrent angular measurements to a point from multiple vantage points. Any underwater can be used, from inexpensive consumer level action cameras, to machine vision cameras in \$1500 pressure housings [52] or even dedicated deepwater equipment, such as the \$60k Sulis subsea camera [58], any of the DeepSea Power & Light equipment [14] or Sidus cameras and lighting solutions [55]. Since stereo algorithms depend on detecting features of the environment, the barren seafloor can pose a challenge [37]. Nevertheless, stereo vision has been demonstrated in a natural environment at 1750 m [7]. Underwater stereo based SLAM has also been demonstrated [47], but low visibility remains an issue. Though few authors report maximum range, 10 m seems to be a good estimate based on qualitative inspection of the visual results in [47].

Structure from Motion (SfM) approaches find the 3D structure of an object through angular measurements from a great number of overlapping but unknown vantage points. They are closely related to stereo methods, also requiring significant processing. Again, any underwater camera can be used. Conventional SfM methods have been used to map coral reefs [9] and in general aquatic applications of the technology are regarded to be rapidly developing [11]. Difficulties in detecting features on the barren seafloor can again pose a challenge, but can ultimately be overcome such that underwater monocular SLAM has been demonstrated [37]. SfM approaches suffer the same limitations as stereo methods.

Structured light scanning uses a light source with a known angular distribution and measures the angles of the reflected light. Laser line scanners are common underwater structured light scanners. Examples include the Newton M310UW [38], the Kraken SeaVision [46] and the 2G Robotics ULS-500 pro [1]. Thanks to the use of laser light, excellent resolutions can be obtained down to  $0.0057^\circ$  (SeaVision). In clear water, the range is limited to 20 m (ULS-500 pro), though usually lower at 5 m (M310UW) or 8 m (SeaVision). To obtain the long range, the trade-off between low volumetric backscatter and sensor to light distance makes for a bulky 1.2 m system (ULS-500 pro). Fighting the trade-off between sensor size, sensitivity and resolution likely contribute to high system cost, \$200k for the ULS-500 pro for example. Some systems, such as the ULS-500 pro are dynamic scanners, such that they rely on the movement of the vehicle for one of their scan axes. This makes them unsuited as a sole sensor for SLAM, though still usable in the more common fusion approach.

ToF systems can be further divided based on the domain of the echo. Sound Navigation And Ranging (SONAR) systems use acoustic echos, LiDAR systems use optical echos and Radio Detection And Ranging (RADAR) systems use radio echos.

RADAR is not suited for underwater use as the signal simply attenuates too fast in water to obtain usable results. For frequencies high enough for practical antenna sizes, the attenuation of radio waves in seawater is too high to perform medium distance ranging ( $>1$  m), due to the combination of the conduction losses at low frequencies [4] and the attenuation of pure water at high frequencies [51]. This makes underwater RADAR unfeasible.

SONAR widely employed for underwater scanning, since its range is not limited by the turbidity of the water. Edgetech [16], Klein Marine [54], Coda Octopus [12], Trittech [64] and Teledyne [59] all produce a multitude of marine SONAR systems. Two SONAR techniques that are often employed are multibeam and side scan SONAR. Multibeam sonar uses phased arrays to steer the laser beam. There is also side scan SONAR. A SONAR beam orthogonal to the direction of motion of the vessel, is combined with a simple altimeter to form a map. SONAR does have its limitations. [20] points out that side scan sonar does not really provide 3D information, since the reflection intensity depends on the orientation of the surface, rather than the distance. The researcher mentions that for practical transducer sizes, the angular resolution remains limited due to the relatively large wavelength of the sound waves. For example, the \$25k Teledyne blueview has a resolution of  $1^\circ$  at a range of 10 m with up to 1 Hz update rates. The \$200k Coda Octopus Echoscope 4G boasts beam spacing down to  $0.19^\circ$  and at a range of 20 m with up to 20 Hz update rates. The Trittech Gemini 720ik has resolution of  $0.25^\circ$  at a range of 1 m and an absurd 97 Hz.

To the best of our knowledge, only one company offers underwater LiDAR. 3DATDepth has designed a \$500k underwater LiDAR system that has a range precision of 6 mm and an angular resolution of less than  $0.025^\circ$ . The maximum range is limited to 45 m [15]. Some authors also distinguish the INSCAN system by Teledyne CDL [17], but the 3DAT-Depth optical stage seems to have been used [29]. Thanks to the short optical wavelengths, the resolution of LiDAR is higher than SONAR. However, the scan rate is too low for SLAM applications at  $2 \text{ min}^{-1}$ . Furthermore, the range is limited by turbidity. Nevertheless, LiDAR systems can assist in increasing efficiency of bathymetry surveys, though cost remains a limiting factor [17].

Further variations are found by combining these methods. For example, Pulse Gated Laser Line Scanning (LLS) employs range gated imaging to reduce interference from backscattering in a structured light scanning method [10].

In conclusion, each underwater ranging method comes with its unique detractors. All solutions in industrial use are either expensive or very expensive. Many are inherently depth-limited because of their reliance on pressure vessels. LiDAR systems are certainly not a solution to all underwater SLAM problems, but given their prominence in regular robotics, they deserve more exploration. Low cost is an especially attractive property. A significant part of the cost of current systems can be attributed to the pressure vessel [17], which can be omitted by using pressure tolerant design techniques [39]. For these reasons, the remainder of this thesis will focus on determining the feasibility of a deep sea SLAM capable pressure tolerant LiDAR system by facing the design challenge.

## 2.2. A simple LiDAR system

Having motivated the choice to investigate deep sea capable LiDAR as a potential solution to the deep sea SLAM problem, we will now examine a simple LiDAR architecture to provide sufficient context to perform more abstract analysis in later sections.

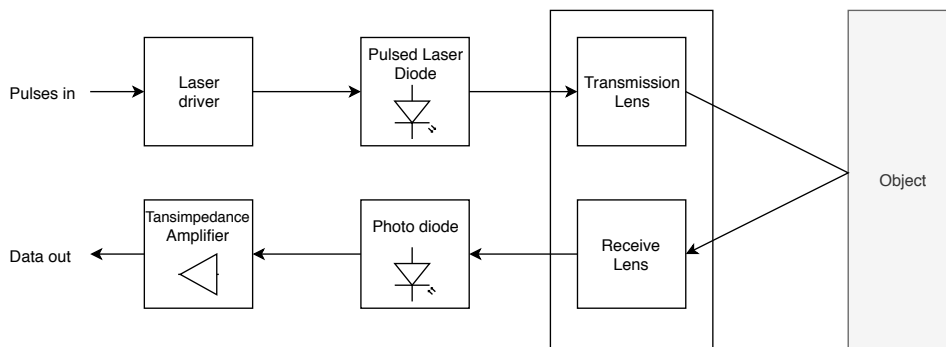


Figure 2.2: Schematic view of a simple LiDAR system, adapted from [61]

A general overview of a simplified LiDAR system can be seen in figure 2.2. The basic concept of a LiDAR system is to send out a pulse of light and measure the time it takes for the pulse to return. Assuming the propagation speed of light is known, a distance can be calculated from this time of flight. Since light spreads and attenuates over distance, the reflection is very weak. Detection is usually aided by sending out a very bright flash of light. The light is also commonly focussed to a tight, collimated beam. This ensures that all the light is reflected from a single target of interest. Laser diodes are commonly used as a means of providing fast light pulses. In most cases, a wavelength is chosen that is not dominantly present in sunlight. This minimises interference.

Generally, the creation of a light pulse is preceded by a timing system generating a pulse with the correct width and at the correct time. This signal generally does not have the signal strength to power the laser, so a laser driver is used. It amplifies the incoming pulses so that the laser diode receives sufficient power to shine brightly. When the light leaves the system, the light gets focused by a lens to obtain a collimated beam. The entire LiDAR system is usually rotated to scan the beam the environment using a gimbal. This ensures that a depth map can be built of the environment - not just a single point.

Once the laser beam hits an object, a small portion of light will reflect back towards the LiDAR system. The light that returns to the LiDAR system will then usually be focused on a photo-diode by a second lens. The photo-diode will produce a small current, which depends on the intensity of the light that hits the photo-diode. This signal is passed through a transimpedance amplifier for further processing. Often, a comparator is used to check whether it passes a certain threshold. If so, a target detection is considered to have taken place and the time is stored. This is then compared with the time the pulse was sent to find the time of flight.

## 2.3. Functions of LiDAR systems

We will now generalise the functions encountered in the simple LiDAR system described in the previous section to extract the more abstract functionalities of LiDAR systems, which will enable us to start defining requirements in the next section. We will only consider standard ranging LiDAR, not doppler LiDAR [6] or imaging LiDAR [19, 43].

### 2.3.1. Channel estimation and target detection

From an abstract view for the simple LiDAR system described in section 2.2, sending out a pulse and checking whether the return signal passes a certain threshold is not one operation, but two. The first is the estimation of the backscatter impulse response of the optical channel, which is the received response after sending out a light pulse. The second is the detection of an obstacle from this impulse response. This is accomplished by determining whether the estimated backscatter impulse response is larger or higher at a certain location using the comparator.

Though this additional distinction may seem arbitrary, it enables the classification of many LiDAR technologies, as we will show in section 2.5. It also allows convenient mathematical description, as shown in section 2.8.

### 2.3.2. The abstract channel & sample distribution

Until now, we have assumed that an optical channel is given, but in the simple LiDAR system described previously, it is determined by gimbaling the LiDAR device such that the optical channel spans different parts of the environment. In a more abstract sense, this is a method to distribute the various distance samples over space. This is required in any 3D LiDAR system, since electrical signals are modelled as 1-dimensional quantities, whilst the environment is a 3-dimensional space. The distribution of measurement samples is thus the problem of splitting the 3-dimensional environment in 1-dimensional channels. The impulse response of the optical channel then becomes a function of the volumetric optical properties of the environment and a steering coefficient vector. It needs to be stressed that this channel need not necessarily be a simple linear trans-section of the environment, but could just as easily be a superposition of these.

### 2.3.3. Towards an FBS

In summary, measuring the distance to the environment by estimating the optical ToF has three facets:

- representing the 3-dimensional environment in 1-dimensional channels, since only these can be transduced to the inherently scalar electrical signals;
- optical channel estimation, where the backscatter of the channel over distance is estimated;
- target detection, where the location of this target is detected on the basis of the estimated channels.

Channel estimation is an experiment on the channel. This requires the emission of test signal into the channel and the reception of the return signal. Furthermore, like all systems the system needs to interface to a user and needs to preserve itself to be useable. This motivates the FBS in Figure 2.3.

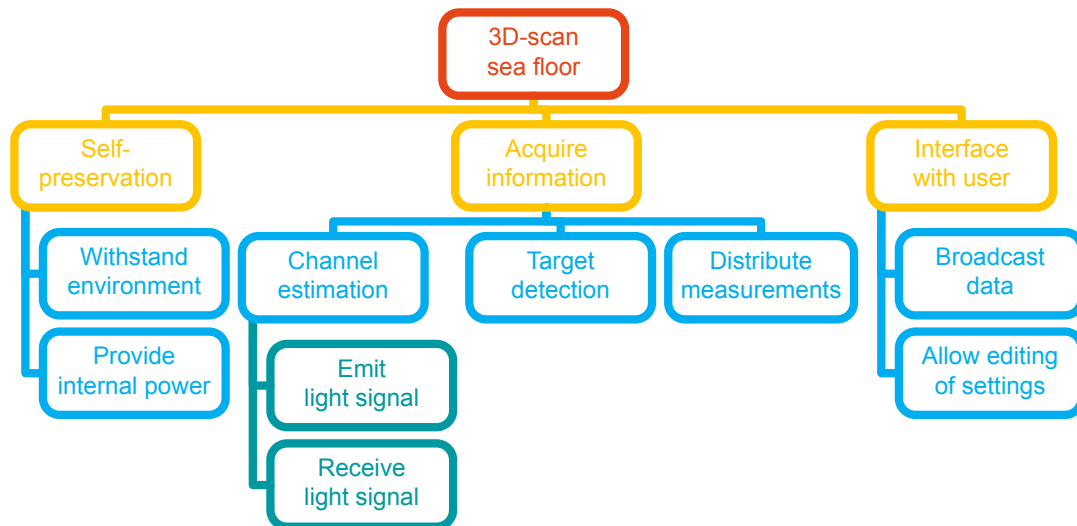


Figure 2.3: LiDAR FBS.

## 2.4. Requirements

### 2.4.1. Towards a RDT

In order to obtain an exhaustive list of requirements for the system, we constructed a RDT, which will serve as the basis of the upcoming programme of requirements. This entailed finding system-wide performance aspects for each

abstract function of the system defined in the FBS discussed in the previous section. The resulting RDT can be found in figure 2.4.

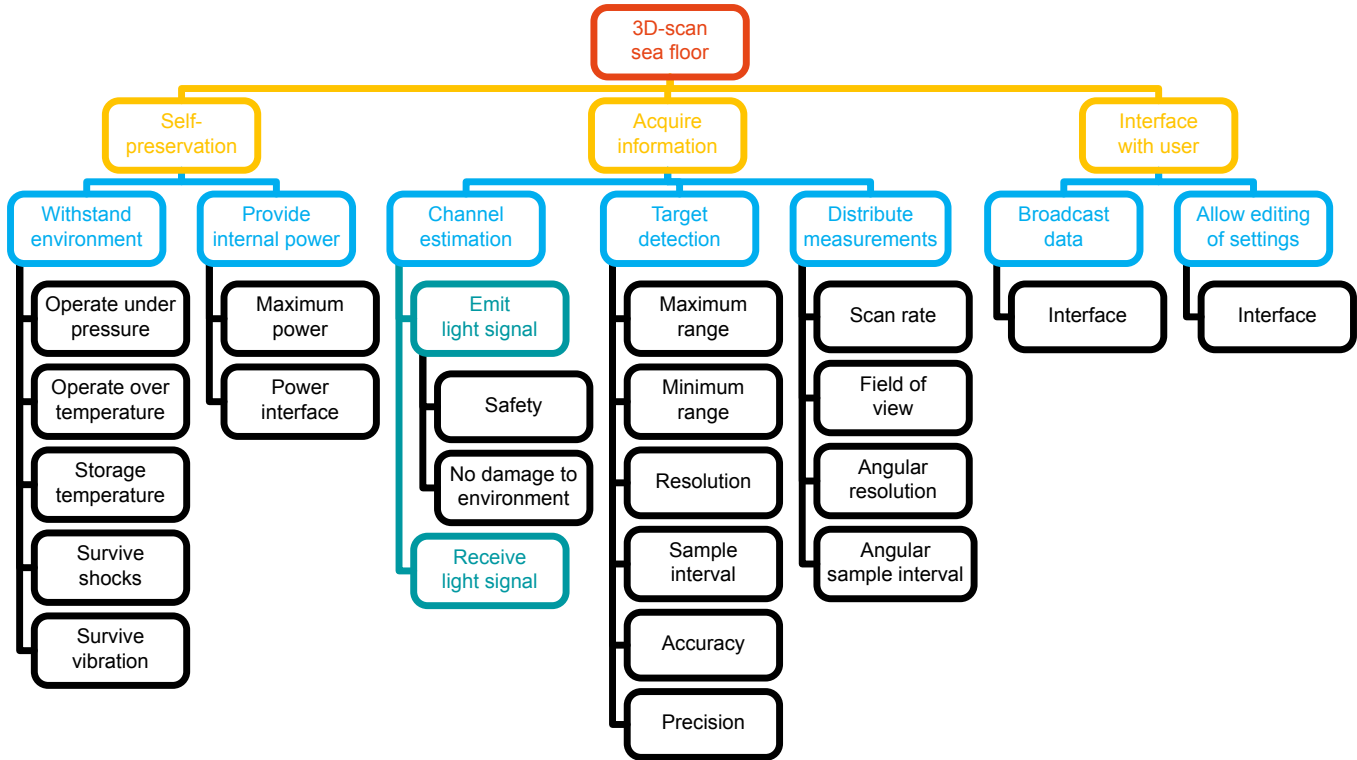


Figure 2.4: SLiDAR RDT.

### 2.4.2. Programme of Requirements

The functions found in the FBS, the requirements found in the RDT and the constraints on the project, form the basis of the program of requirements, which will enable judging of the suitability of design options to form a concept design in later sections. We quantified the requirements based on our market research (part of which is represented in section 2.5) and estimations of the performance required for SLAM. Most of the obligatory requirements were roughly quantified based on an inexpensive triangulating laser scanning system found on entry-level SLAM capable systems, the RPLidar-A1 [57]. The more ambitious goals are based on the unique and high end SL3 underwater LiDAR from 3DAtdDepth [15] and the Velodyne Puck [65], which has been a standard for research into the application of SLAM to self-driving vehicles. Further detailing yielded the programme of requirements on the system shown in table 2.1. We have given each requirement a unique identifier for reference throughout this thesis. We have also given our justification for including the requirement or the value of the requirement for future reference. Finally, we have indicated how the requirement is to be verified as a first step in the creation of verification plans.

Table 2.1: System-wide requirements and justification

ID	Requirement	Verification	Justification
FUN1	The system shall estimate the distance to the environment by measuring the optical time of flight at certain sample points within a certain angular region.	• Test Demonstration Analysis Inspection	Basic functionality of a LiDAR.
FUN2	The system shall be able to stream this measurement data via a serial data protocol.	•	Enables use of the system.
FUN3	All variable parameters should be user-configurable over the serial data protocol.	•	Increases flexibility of the system.
ENV1-a	The system and its internals shall operate in compliance with the requirements up to a pressure of 100 bar.	•	Test limit of MacArtney pressure chamber.
ENV1-b	The system and its internals should operate in compliance with the requirements to a pressure of 600 bar.	•	Test limit of AWI pressure chamber.

Continued on next page

Table 2.1 – Continued from previous page

ID	Requirement	Verification			Justification
		Test	Demonstration	Analysis Inspection	
ENV2-a	The system shall operate in compliance with the requirements in a temperature range between $-10^{\circ}\text{C}$ and $50^{\circ}\text{C}$ .		•		Minimum and maximum ocean water temperatures, with margin.
ENV2-b	The system shall survive temperatures in a range between $-60^{\circ}\text{C}$ and $70^{\circ}\text{C}$ .		•		Minimum and maximum atmospheric temperatures, with margin.
ENV3	The system should survive shocks.	•			In case the robot bumps into obstacles.
ENV4	The system should survive vibrations.	•			To avoid damage from thruster vibrations.
SAF1	The system shall comply with the intent of the IEC60825 safety standard.		•		Ensure team safety.
INF1	The system will receive a 48 V connection.			•	LOBSTER Explorer bus connection.
INF2	The system shall draw no more than 100 W.		•		Sufficiently low power for the LOBSTER Explorer.
INF3-a	The system shall be able to communicate over an Serial Peripheral Interface (SPI) bus.	•			Simple yet high speed and versatile interface.
INF3-b	The system should communicate over a 100BASE-TX Ethernet link or faster.	•			High-speed interface of the LOBSTER Explorer.
PER1-a	The system shall have a maximum range of at least 10 m in 95% transmissive ocean water in a typical ocean environment.	•	•		Braking distance with margin of LOBSTER Explorer.
PER1-b	The system should have a maximum range of at least 40 m in 95% transmissive ocean water in a typical ocean environment.	•	•		Range of commercial systems.
PER2-a	The system shall have a minimum range less than 1 m.	•	•		Braking distance with margin of LOBSTER Explorer.
PER2-b	The system should have a minimum range less than 0.05 m.	•	•		Range of commercial systems.
PER3-a	The system shall have a distance resolution of less than 5 cm.			•	Estimated minimum required for SLAM.
PER3-b	The system should have a distance resolution of 1 mm.			•	Resolution of commercial systems.
PER4-a	The system shall have a distance accuracy of a standard deviation of 5 cm.	•			Estimated minimum required for SLAM.
PER4-b	The system should have a distance accuracy of a standard deviation of 1 mm.	•			Accuracy of commercial systems.
PER5-a	The system shall have a distance precision of 1%.			•	Precision of commercial systems.
PER5-b	The system should have a distance precision of 100 ppm.			•	Estimated minimum required for SLAM.
PER6-a	The system shall have a minimum Field Of View (FOV) of $30^{\circ} \cdot 30^{\circ}$ .			•	Estimated minimum required for SLAM.
PER6-b	The system should have a FOV of $180^{\circ} \cdot 90^{\circ}$ .			•	FOV of commercial systems.
PER7-a	The system shall have a maximum azimuthal sample interval of $1^{\circ}$ .			•	Estimated minimum required for SLAM.
PER7-b	The system should have a maximum azimuthal sample interval of $0.1^{\circ}$ .			•	Azimuth sample interval of commercial systems.
PER8-a	The system shall have a maximum zenithal sample interval of $15^{\circ}$ .			•	Estimated minimum required for SLAM.
PER8-b	The system should have a maximum zenithal sample interval of $0.1^{\circ}$ .			•	Zenith sample interval of commercial systems.
PER9-a	The system shall have an angular accuracy better than $1^{\circ}$ .	•			Angular accuracy comparable to minimum angular resolution.
PER9-b	The system should have an angular accuracy better than $0.1^{\circ}$ .	•			Angular accuracy comparable to maximum angular resolution.
PER10-a	The system shall have an angular precision better than $1^{\circ}$ .	•			Angular precision comparable to minimum angular resolution.
PER10-b	The system should have an angular precision better than $0.1^{\circ}$ .	•			Angular precision comparable to maximum angular resolution.
PER11-a	The system shall have an maximum update rate of at least 10 Hz.			•	Estimated minimum required for SLAM.
PER11-b	The system should have an maximum update rate of at least 30 Hz.			•	Update rate of commercial systems.
PER13-A	The size of the system shall fit in the mechanical design of the LiDAR			•	As presented by the team of mechanical engineers [48]
PRO1	The project shall be completed by June 21th of 2019.			•	Requirement from BAP.
PRO2	The project shall be documented according to the Electrical Engineering BAP guidelines.			•	Requirement from BAP.
PRO3	The project shall be completed by a team of 6 3rd year bachelor students.			•	Requirement from BAP.
PRO4	The development and fabrication of the electrical system shall cost no more than €3000.			•	Budget.
PRO5	The mechanical scanning stage, optics and embodiment will be developed by a BEP team of mechanical engineers.			•	Agreement with the BEP team of mechanical engineers.

## 2.5. Design options

Having defined the functions of and requirements on our deep sea LiDAR system, this section aims to explore aspects of LiDAR system architectures which fulfil these so that they can be considered as design options for the concept design. To this end, we examine the current state of the art LiDAR techniques along with their merits and weaknesses.

We have organised the techniques by the function they implement to emphasise their commonalities and differences. After considering various solutions for distribution, channel estimation, target detection and digitisation, we summarise these in a DOT for further reflection.

### 2.5.1. Distribution

There are two main approaches to implement the distribution of samples over space:

- scanning systems, where a single measurement beam is rotated over time so that consecutive samples cover different directions;
- concurrent sampling or scannerless systems, where multiple directions are sampled concurrently.

#### Gimballing systems

The advantage of scanning systems is that they make efficient use of the relatively expensive ToF estimation ('laser profiling') hardware. Hence, when LiDAR technology was first developed, only scanning systems were economically feasible. Early scanning systems were mechanical in nature, gimballing the entire laser profiling assembly. The advantage of gimballing is that light beams always enter the receiver from the same angle, simplifying the optical path and ensuring that the effective reception area is constant over any beam deflection  $\phi$ . For these reasons, this method still enjoys widespread use today, primarily in 'spinning LiDARs', which rotate over a single axis. Examples include [42, 65, 56]. There is the disadvantage of requiring connections over one or more rotating axles. This is solved either using slip rings, which are widely considered unreliable and which are unsuited for high-speed data transfer, or using coupled coils for power and optical transmission for data [30], which add complexity.

#### Polygon scanners

Polygon scanners are another mechanical scanning method, where a rotating mirror is used to direct the beam over the FOV [31]. Irregular polygon scanners even enable scanning in the vertical direction by angling each face of the polygon over an axis orthogonal to the rotation direction [31]. These decouple the scanning and laser profiling, but they introduce a Trade-off between the maximum FOV and the amount of vertical samples. They can be used with a separate, fixed reception stage, but this would decrease the effective reception area with  $\cos(\phi)^2$  for samples towards the edges of the FOV. In contrast, it is possible to use the mirror as the return path for the light [27]. In this case, the mirror is at an angle of  $\phi/2$  to the returning light, such that the effective reception area decreases with  $\cos(\phi/2)^2$  towards the edges of the FOV.

#### MEMS micromirrors

MicroElectroMechanical Systems (MEMS) micromirrors are tiny oscillating mirrors used to direct the the beam over the FOV [66]. Their small size is an advantage, though the aperture size and resonant frequency are at odds with each other [35]. They are often driven at resonance to extend the FOV, but when used in liquids, their frequency response is damped such that this is no longer possible and their scan frequency reduces by an order of magnitude from typical 300 Hz to 30 Hz [70, 67].

#### Optical Phased Arrays (OPAs)

With the advent of autonomous driving, manufacturers want to increase the reliability of scanning methods, generating interest in solid-state scanning methods. One of these is the optical phased array, where the beam is composed of a superposition of many smaller beams with tunable phases, resulting in a steerable beam [45]. Advantages include high scan speed, small size and high reliability, but the technology is still in its infancy and thus very expensive, in academia [35] and in industry [41].

## Scannerless versus scanning systems: merits and weaknesses

Thanks to modern advances in miniaturisation, scannerless systems have become viable. The advantage of scannerless systems is that they have a greater scan time per sample, so that the same pulse energy can be achieved using lower peak power illumination. In addition, when limited by eye-safety, longer pulses are permitted higher pulse energies. However, macroscopic mechanical scanning methods and especially spinning LiDARs have the advantage that different pulses are emitted in different positions, such that only a fraction of the total emitted flux flows through an eye-sized area. This means that the pulse energy can be increased [63]. All scanning systems have the advantage of being able to incorporate more refined laser profiling hardware, since cost and effort do not have to be shared over multiple channels but can be focused in a single channel [35].

### Scannerless arrays

Perhaps the simplest is creating an array of differently directed laser profilers operating simultaneously, as demonstrated by Ouster in [44]. They show that laser emitters can be integrated on a single Integrated Circuit (IC) using Vertical Cavity Surface Emitting Laser (VCSEL) technology. Advantages include high reliability and low system complexity. Scannerless arrays are often referred to as 'flash multibeam LiDAR'. In this, 'flash' denotes the simultaneous capture of multiple samples, like in a camera sensor illuminated by a flash, and 'multibeam' denotes the multiple targeted beams of light, only illuminating the environment where sampled [44].

### Diffuse source

Instead of replicating directed light sources with each laser profiler in an array, a single diffuse light source can be used [33]. This technique is often referred to as 'flash LiDAR', since multiple samples are captured simultaneously using the same flash of light. Shorter-range systems meant are also referred to as ToF cameras [18]. The advantage is lower system complexity, however much will fall on areas of the environment which are not sampled. Since the total luminous flux flows through a single eye-sized area, the energy of the flash is limited by eye-safety. Then this limits the effective pulse energy at each sample location compared to systems incorporating transmitter arrays.

### Coded aperture

One intriguing possibility is to use Compressed Sensing techniques to reconstruct a scan from samples of a small amount of select beam patterns. A few investigations have been carried out on coded aperture LiDAR [23] and [53]. Both systems send out a diffused source and capture the returned signal with multiple sensors. In comparison with flash LiDAR, less sensors could be used if a static coded aperture is used, this would reduce the cost significantly. Although most literature on compressed sensing does not discuss the effect of noise introduced to the signal before detection, it has been proven that in some cases the signal to noise ratio decreases due to noise folding [3].

## 2.5.2. Channel estimation

The complexity of optical channel estimation techniques is limited due to the required high operating speed. Because of this, only matched filter approaches are commonly implemented and the possible application of modulation is the main difference between these techniques. We will now consider the most common modulations.

### Single pulse

Single pulse LiDAR, or 'pulsed' LiDAR, is perhaps the simplest modulation, and certainly very common in industry [25]. With it, a single pulse high-intensity pulse is emitted each sample [61]. Since the pulse can be modelled as a bandwidth-limited delta pulse, the matched filter is simply a low-pass filter, which is inherent to any input stage. Pulsed illumination can also be easily achieved using a push-pull driver, such that the output stage can be very simple. In short, simplicity is the main advantage of single pulse LiDAR, and it is certainly prevalent in scannerless systems. This simplicity does come at the cost of a relatively large susceptibility to external disturbances. Since all energy is concentrated in a single peak, the pulse energy will be limited by the peak power of the electro-optical transducer, which may be low. Furthermore, at short pulse lengths only low pulse energies are considered to be eye-safe.

### Harmonic

Some time of flight cameras use a harmonic signal<sup>1</sup> for channel estimation. In this case, the time of flight is calculated from a relatively simple phase shift measurement [26]. The advantage is that the usual complexities of high speed ToF

<sup>1</sup>A square is often used for simplicity, but the input signal is typically thresholded, such that the square wave can be regarded as the binary equivalent of a sine wave.

estimation can be avoided, since only low-speed amplitude measurements are required. However, usually a harmonic signal would not even be considered for channel estimation. This is because due to the tiny bandwidth, all objects in the channel will alias on top of each other. Thankfully, objects farther away in the channel generate weaker returns due to  $R^{-2}$  spreading. Combined with the small spot enabled by the optical extremely high frequencies exploited by LiDAR this makes the nearest return dominant, which is usually the only return of interest. However, it is impossible to distinguish a dominant return from a dominant return at a length  $c \cdot f/2$  further away, since both alias to the same point. Hence, the domain of harmonic channel estimators is usually limited to  $[0, \cdot f/2)$  in order to prevent these range ambiguities. Though this limit could be overcome by using a select few frequencies, any amount of near-field volumetric backscatter due to the environment could become the dominant return at longer ranges due to higher  $R^{-2}$  spreading. Hence, harmonic channel estimation is usually reserved for short range indoor use in time of flight cameras.

## FMCW

Frequency Modulated Continuous Wave (FMCW) systems continuously transmit a frequency modulated light wave. This modulation enables a Continuous Wave system to be used for distance measurements. The distance measurement for FMCW is done by comparing the received signal with a reference signal [28]. The distance between the source and the reflecting object can be calculated as  $R = c_0 |\Delta t|/2$ . Here  $\Delta t$  is the measured delay time between the reference and the received signal. An inherently high SNR makes this technique advantageous. A disadvantage is the need of high bandwidth to increase the maximum ranging distance, and the need for a heterodyne receiver.

## Pulse trains

In pulse train implementations, multiple pulses are sent for every distance sample. The received signals are then averaged for higher Signal to Noise Ratios (SNRs). Correlation processing is then used to find the ToF [24]. The advantage of a pulse train is that the total pulse energy is spread over many pulses with an equivalent bandwidth, such that the peak power can be reduced. The downside is that in low SNR regimes, the nonlinearity of detection methods cause noise standard deviation after detection to grow superlinearly as a function of noise standard deviation before detection. Because of this, the pulses must be averaged before detection. This either requires expensive full digitisation of the amplitude of the pulses or complex analog filters.

### 2.5.3. Target detection

As with channel estimation, the complexity of optical channel estimation techniques is limited due to the required high operating speed. We will now consider the most common techniques.

#### Static thresholding

The simplest technique is static thresholding, where the return signal is compared to a constant threshold [61]. A target detection is recorded when the signal passes this threshold. The advantage is the simplicity, but the disadvantage is that the method is unreliable in the presence of volumetric backscatter. In that case, backscatter from scattering media close-by will be brighter than returns from faraway legitimate targets, due to the attenuation of light over distance. In air, this usually is not a problem, since it is a near-perfect medium. However, bad weather such as mist can interfere with this detection method [68].

#### Adaptive thresholding

The susceptibility of static thresholding implementations to volumetric backscatter can be overcome by adapting the threshold over time or based on the returned signal. Examples include Constant False Alarm Rate (CFAR) detectors, which adapt the threshold according to a function of the background surrounding the sample and also more complex Bayesian methods [40]. The main advantage is lower susceptibility to volumetric backscatter, but the approaches are noncausal and may require sophisticated processing (Bayesian methods). This either requires expensive full digitisation or complex analog filtering.

### 2.5.4. Digitisation

The incoming light is converted to an analog electrical signal, but most LiDAR systems provide their ToF estimates digitally. Hence the signal must be digitised in order for the digital part of the system to properly process the information. Different types of digitisation techniques were considered for the design of the LiDAR and will be discussed in the forthcoming sections.

## Analog to Digital Converter (ADC)

An ADC (as the name entails) fully converts the analog signal to a proper digital signal. They are often used in systems which fully digitise the light intensity signal. An advantage of ADC based implementations is the lower analog complexity, as complex signal processing can be implemented in software. Another advantage of an ADC implementation is the potential of acquiring volumetric density information about the 3D space, which could be of interest to the user. However, due to the high bandwidth required for LiDAR applications, sufficiently capable ADCs tend to be expensive. Also, the dynamic range of these high-speed ADCs is often insufficient for LiDAR applications, so the input dynamic range must be compressed using either nonlinear circuits [5] or time-variant amplifiers [2].

## TDC

Time to Digital Converter (TDC) is a device which reads out a digitised time interval between two rising edges [8]. Advantage of a TDC are the conceptual simplicity and low cost. The disadvantage is that a TDC based implementation forces signal processing to be implemented in analog electronics, increasing complexity. Another disadvantage is that the output data is only the distance to a target and thus no other information about the channel can be acquired such as target strength or multiple returns.

## Phase measurement

In phase measurement digitisation, the time of flight is found by comparing the accumulated electrical of the normalised received pulse while the system was transmitting  $Q_1$  and the accumulated normalised received electrical charge while the system is not transmitting  $Q_2$ . From these, the distance is calculated using equation 2.1.

$$d = 0.5 \cdot c \cdot \Delta t \cdot \left( \frac{Q_1}{Q_1 + Q_2} \right) \tag{2.1}$$

The advantage of this method is the simplicity, and it is often used in ToF cameras [26]. The major disadvantage is the susceptibility to volumetric backscatter. The returned pulse is required to be either fully on or fully off for processing, which entails thresholding. However this threshold is difficult to define in the presence of volumetric backscatter, as explained previously.

## 2.5.5. Design Option Tree (DOT)

We will now present a short visual summary of the high-level design options for LiDAR systems discussed so far in the DOT shown in figure 2.5. This will serve as an accessible reference for the upcoming concept selection.

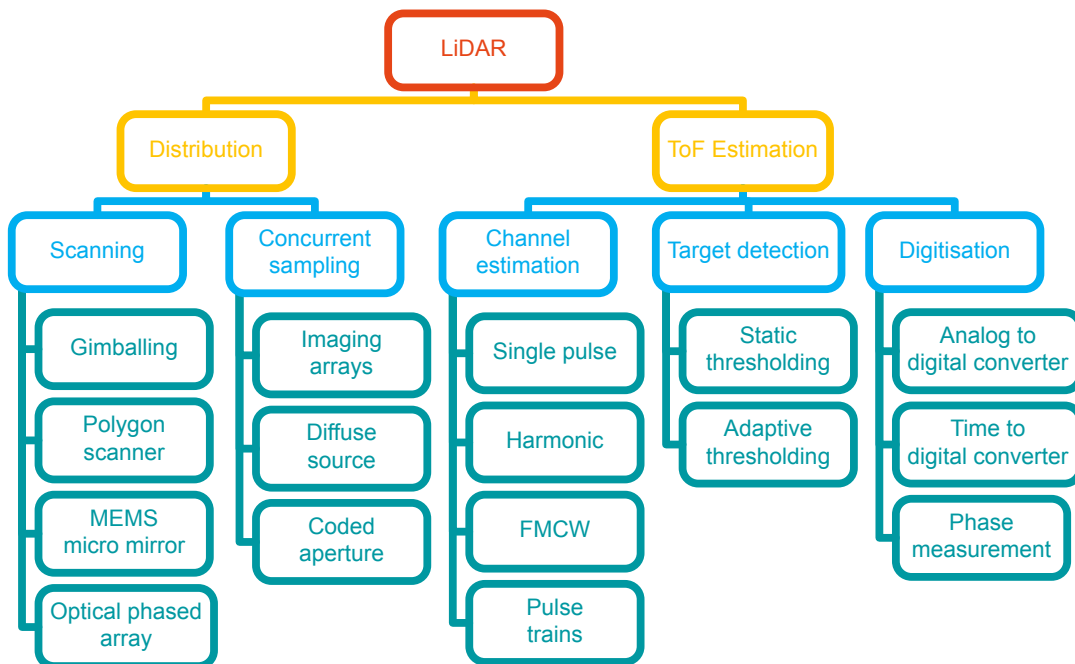


Figure 2.5: High-level LiDAR DOT.

## 2.6. Concept selection

In this section, all of the discussed design concepts for each part of the LiDAR system are weighed in upon. Given the criteria for each part, a decision is then made as to which design concept is most suitable for each part of the LiDAR. In the forthcoming sections, the decision for each part of the LiDAR is discussed.

### 2.6.1. Distribution

Table 2.2 illustrates the advantages of the different distribution methods. Based on the criteria given in the table, it was decided to implement a polygon scanner for the distribution system, since we only considered its implementation to be time feasible.

Table 2.2: Trade-off table for the distribution

	Distribution							Explanation
	Gimball	Polygon	MEMS	OPA	Array	Diffuse	Coded	
Size	±	-	+	+	+	+	±	Size should comply to requirement <a href="#">PER13-A</a>
Fluid Function	±	±	-	±	+	+	-	The system will be fluid-filled as per <a href="#">ENV1-a</a> and <a href="#">ENV1-b</a>
Implementation time	±	+	±	-	±	±	-	Development time is limited, as per <a href="#">PRO1</a>

### 2.6.2. Channel estimation

Table illustrates 2.3 channel estimation trade-offs. We decided to use the single pulse technique based on since it had the best feasibility per [PRO1](#) and [PRO3](#) at an acceptable range to satisfy [PER1-a](#) and [PER1-b](#).

Table 2.3: Trade-off table for the channel estimation method

	Channel estimation				Explanation
	Single	Harmonic	FMCW	Pulse train	
Modulation	+	+	-	±	Simplicity of the modulation technique
Detection	+	±	-	±	Complexity of the detection method
Range	±	-	+	+	Maximum range that can be achieved

### 2.6.3. Digitisation method

For the digitisation method, it is of utmost importance to minimise the noise in the received signal and implementation complexity. For the options that were considered for the LiDAR, it is important to discuss the quality of information versus the complexity of the implementation. Table 2.4 illustrates the advantages for each digitisation method. In order to maintain feasibility as per [PRO1](#) and [PRO3](#) at the decision was made to implement a TDC for the digitisation since it can be validated the quickest.

Table 2.4: Trade-off table for the digitisation technique

	Digitisation			Explanation
	ADC	TDC	Phase	
Complexity	±	-	-	Complexity of the implementation
Flexibility	+	-	-	Flexibility of the implementation with the other devices
Time to prototype	-	+	-	Time to first test of the simplest iteration

### 2.6.4. Target detection

When choosing a target detection technique it is of importance to keep in mind that the operating environment is sea water. The trade-offs between static and adaptive target detection can be found in table 2.5. Though the adaptive target detection is very complex, its resilience against backscatter is of the utmost importance. Since static detection would give too many spurious detections to meet PER9-a and PER9-b, it was decided to implement adaptive detection, despite the additional complexity, possibly interfering with PRO1 and PRO3.

Table 2.5: Trade-off table for the target detection techniques

	Target detection		Explanation
	Static	Adaptive	
Complexity	+	-	Complexity of the implementation
Flexibility	±	±	Flexibility of the implementation with the other devices
Reliability	-	+	Reliability in the presence of close-by scattering media

### 2.7. Subsystem selection

As described in the overview of a simple LiDAR in section 2, a transmit stage consisting of a laser diode together with a laser driver are necessary to convert an arbitrary timing signal to a laser pulse that leaves the system. Also, a receiving stage consisting of a photo diode, together with the necessary data processing was needed to in fact retrieve the light and process the data. The focusing of the beam is not considered in the scope of the electrical part of the SLiDAR because this is mainly a mechanical issue. The system described in section 2 does not have any form of beam steering and can thus only measure one point. However, the SLiDAR has to measure multiple points in space, thus some sort of beam steering has to be implemented. Furthermore, The data has to be processed and all actions, such as choosing a point in space to measure the distance or sending out a laser pulse, have to be coordinated. This is why we came to the following subsystem division.

- A transmitting stage
- A receiving stage
- A beam Steering stage
- A Data processing stage

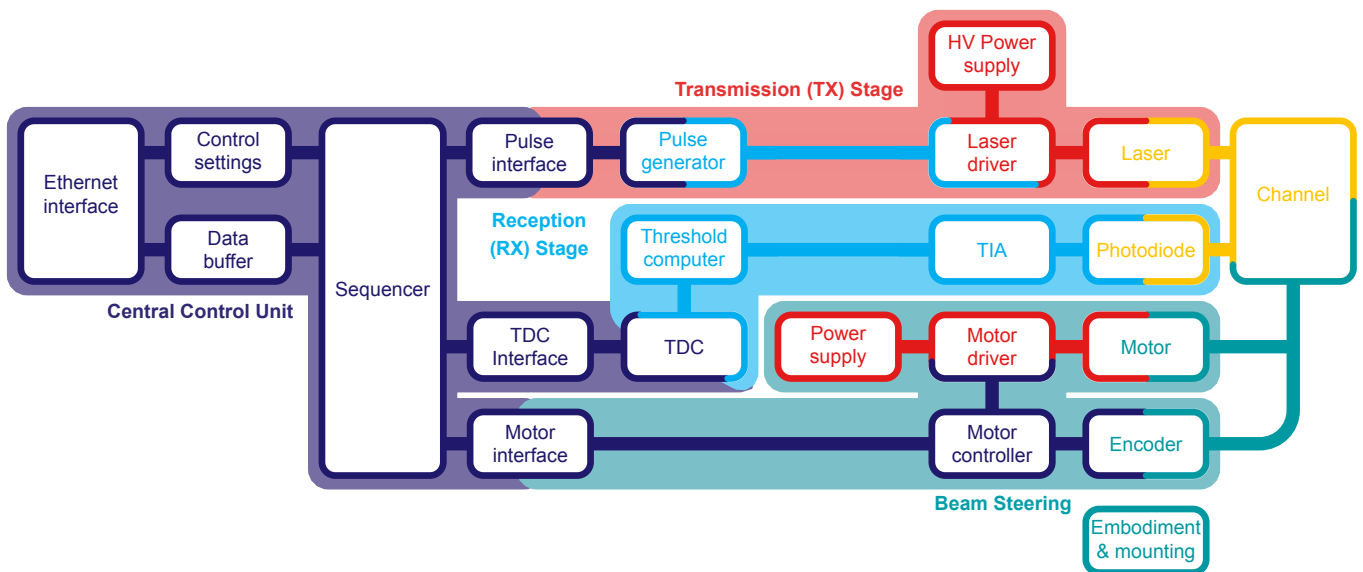


Figure 2.6: Low-level system architecture. Digital is purple, analog signal processing is cyan, high power is red, optical is yellow and mechanical is green. Modules converting domains are a mix of colours.

## 2.8. System modelling

The subsystem division generates requirements on the interfaces of subsystems. Two important interfaces is the interface of the transmission stage to the optical channel and the channel to the reception stage. These take the form of the optical output power of the transmission stage, the input sensitivity and input referred noise of the reception stage, the wavelength and the bandwidth of both subsystems. Together, these determine the minimum range, maximum range and distance resolution. In order to dimension these subsystem requirements, their relation to the system requirements needs to be found. In this section, we construct a simplified model of the optical channel to find this relation.

### 2.8.1. Towards a simple model

We have defined a LiDAR device as an apparatus which measures the distance to objects by estimating the optical time of flight to those objects. Then a LiDAR device detects features of its environment. We model the environment as two scalar fields:

- A transmissivity field  $T(\vec{R})$ , which models the amount of light which is not absorbed or reflected when a beam travels through a medium, such that the forward intensity  $\lim_{\Delta\ell \rightarrow 0} I(\vec{R} + \Delta\vec{\ell}) = I(\vec{R}) \cdot T^{|\Delta\vec{\ell}|}$ . It must always have a value between 0 and 1, since we assume that there are no energy sources to amplify the light in the environment.
- A reflectivity field  $\beta(\vec{R})$ , which models the amount of light reflected back at the source at each point, such that the magnitude of the backscattered light is  $I_b = I \cdot (1 - T) \cdot \beta$ . It must also always have a value between 0 and 1.

LiDAR devices can detect only these fields. This is accomplished by characterising one or a variety of optical paths through the medium and applying channel estimation techniques. Other models model the scattering of the beam in space using distribution function [34]. Assuming that multiple backscatter effects are insignificant and using the fact that our system has a coaxial receiver and transmitter, only the amount of light propagating to the next distance segment needs to be considered, and the simplified model suffices.

Sometimes knowledge of these scalar fields is enough. Cloud observations would be complete with complete knowledge of these scalar fields. In other cases, distances to interesting objects must be inferred from these fields. In SLAM applications, one is interested in solid obstacles. Most are characterised by  $T \approx 0^2$ .

Then LiDAR devices must do two things:

- Channel estimation
- Obstacle detection

To constrain the key system parameters, We will now model the channel and the optical signal therein in the context of obstacle detection.

### 2.8.2. Channel impulse response

For a perfectly collimated beam travelling between points  $\vec{a}$  and  $\vec{b}$  the intensity  $I$ :

$$I(\vec{b}) = I(\vec{a}) \cdot \exp\left(\int_{\vec{a}}^{\vec{b}} \ln(T(\vec{R})) \cdot |d\vec{R}|\right)^2 \quad (2.2)$$

We define the magnitude of light reflected back at each position as:

$$I_b(\vec{R}) = I(\vec{R}) \cdot (1 - T(\vec{R})) \cdot \beta(\vec{R}) \quad (2.3)$$

Incorporating  $x^2$  spreading back from the target to the receiver for large  $x$ , modelling optical inefficiencies using a factor  $\eta$ , assuming lambertian reflection and assuming that the full beam is reflected we find for the impulse response in terms of power:

$$p(x) = \eta \cdot \exp\left(\int_0^{x/2} \ln(T(\tau)) d\tau\right)^2 \cdot (1 - T(x/2)) \cdot \beta(x/2) \cdot \frac{A_0}{(x/2)^2} \quad (2.4)$$

In which  $x = u_p \cdot t$ ,  $A_0$  is the effective receiver area.

<sup>2</sup>Glass is an exception, but it is rare in underwater LiDAR applications

### 2.8.3. Towards wavelength requirements

At longer distances, the exponential term in equation 2.4 modelling bulk absorption will start to play a dominant role. The absorption is highly dependent on the wavelength. Hence, a wavelength should be selected such that absorption is minimised. The absorption in different types of sea water is very well classified by Jerlov's water mass classification [36]. This shows that absorption is maximised for a wavelength around 520 nm in type I, II and III oceanic waters. Traditionally, this wavelength would be avoided due to the significant solar irradiance causing interference, but this light does not penetrate to the deep sea. We have detailed this consideration as requirement TX-PER1 in table 2.6.

### 2.8.4. Towards power & input sensitivity requirements

In order to find the required power and input sensitivity, we modelled a maximally absorptive homogeneous channel using  $T = 95\%$  as per PER1-a and PER1-b. We assume that volumetric backscatter is caused by floating particulates of the same material as sediments covering the sea floor, such that  $\beta(x) = \beta$  is everywhere constant at a minimum value of 0.1 based the darkest sediments in underwater reflectance measurements in [69].

A main factor in the attenuation of the transmitted signal, are the optical elements. Firstly lenses always have a small inefficiency, this has to be taken into account. Secondly, focusing the outgoing laser light on the photo detector also greatly influences the received optical power. The mechanical design therefore already introduces some losses in the optical path.

We implemented a Matlab script with our model to find the range associated with input threshold and output power values. We used values given in the reference design [61] as a basis for the the parameters and adjusted to find a reasonable division of requirements, given in table 2.6. The Matlab script can be found in B.

### 2.8.5. Towards bandwidth requirements

The bandwidth is directly related to the outgoing pulse width, so determining the pulse width fully constrains the bandwidth. We will now investigate the effects of changing the pulse width on the channel estimate to find the required pulse width.

In general range finding, the pulse width determines the distance resolution of the system. If objects are closer to each other than the pulse width, they become indistinguishable. Because of the small beam diameters of LiDAR systems, the assumption is often made that all light is reflected by a singular target, such that there is only a single return. However, the backscatter also generates weak returns. Since these returns are distributed over space, the signals ranging between those on the front of the pulse reflected from farther away and the signals on the back of the pulse reflected from shorter away will reach the receiver simultaneously. This generates interference, which scales with pulse width and must be limited. We will now use our simplified model to express this interference in terms of the pulse width of the subsystems to constrain the pulse width.

To find estimate the maximum interference versus distance, we assume clear water before that distance and the most absorptive water thereafter. To simplify calculations, we also ignore the absorption within the length of the channel occupied by the pulse, which will lead to slight overestimation. We can then remove the exponential term from equation 2.4 and correlate with a square pulse to find the maximum interference versus distance in equation 2.5.

$$p_i(x) = 4\eta\beta A_0 \cdot (1 - T_{min}) \cdot \left( \frac{1}{x-L} - \frac{1}{x} \right) \quad (2.5)$$

Any detector should not register a detection at this maximum interference level. This puts a lower limit on the threshold. We can express this by modelling the maximum factor  $\alpha$  that the threshold can be lower to maximum return. This is obtained when  $T = 0$  after clearwater, such that bulk absorption can be ignored. This yields equation 2.6 for  $x > L$ .

$$p_{max}(x) = 4\eta\beta A_0 \cdot \frac{1}{x^2} \quad (2.6)$$

Since  $p_i(x)$  falls superquadratically for  $x \rightarrow \infty$ , there is a range where  $p_i(x_{min}) = p_{max}(x_{min})/\alpha$ . Below this range, it can not be guaranteed whether an obstacle is detected or volumetric backscatter. Solving the equation yields equation 2.7.

$$L = \frac{x_{min}}{(\alpha \cdot (1 - T_{min}) \cdot x_{min} + 1)} \quad (2.7)$$

We assume that  $\alpha = 6$  is a reasonable value,  $T_{min} = 0.8$ , and  $x_{min} = 1$  m per PER2-a or  $x_{min} = 0.05$  m per PER2-b. This gives a pulse width  $L = 0.45$  m per PER2-a, which corresponds to 2 ns and a pulse width of  $L = 0.05$  m per 0.2 ns PER2-b. This corresponds with bandwidths of 0.5 GHz and 5 GHz respectively. These requirements are detailed in table 2.6.

Table 2.6: Subsystem requirements

ID	Requirement	Verification		Justification
		Test	Demonstration Analysis Inspection	
TX-PER1	Light emitted by the transmission stage shall have a wavelength between 505 and 535 nm .	•		Minimises absorbance while allowing slight deviations due to changing operating conditions.
TX-PER2	The optical power emitted by the transmission stage shall have a value higher than 6 W	•		In order to meet the range specifications.
TX-PER3a	The pulse width of the light emitted by the transmission should remain smaller than 2 ns	•		In order to limit the interference.
TX-PER3b	The pulse width of the light emitted by the transmission should remain smaller than 0.2 ns	•		In order to limit the interference.
RX-PER1	The threshold of the RX stage shall be less than 0.05 W.	•		In order to detect at the required range.
RX-PER2a	The bandwidth of the RX stage shall be at least 500 MHz	•		In order to limit the interference.
RX-PER2b	The bandwidth of the RX stage should be at least 5 GHz	•		In order to limit the interference.

## 2.9. Functional Overview

This section serves as a brief overview of the functional operation flow of the proposed LiDAR design from section 2.7. From this overview, the interfaces between subsystems are defined. The reader can use this section to put the design of the subsystems in following chapters into the perspective of the LiDAR system as a whole.

### 2.9.1. Functional flow

A high-level functional overview of a single distance measurement of the proposed LiDAR design is given in figure 2.7. The motor in the diagram rotates the polygon mirror. The direction in which the laser pulse is sent depends on the angular position of this mirror. The angular position is most accurately known when the mirror rotates with a steady-state angular velocity. Hence, the CCU waits for steady-state motor rotation before measurements start.

A distance measurement consists of a number of sequential events. The CCU instructs the Transmission (TX) Stage to send a laser pulse to the measurement channel. The timestamp of this event is recorded by the TDC. A laser reflection comes back from the channel, and is detected by the APD. The Reception (RX) stage converts this detection to a pulse, of which the TDC records the timestamp. The CCU computes a distance estimate from the two TDC timestamps, and streams it to the user via a serial data protocol.

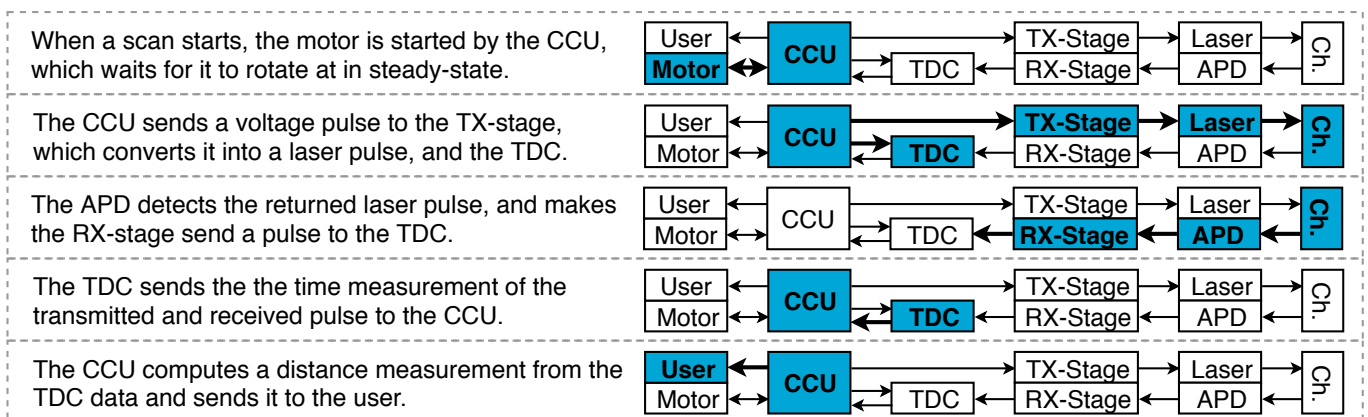


Figure 2.7: High-level functional overview of a single distance measurement. Active parts of the system during a step are highlighted.

Laser pulses are transmitted in packets called frames. The relation between the timing of frame transmission and the rotation of the mirror is illustrated in figure 2.8. When the line of sight of the laser diode crosses a corner of the mirror, the Beam Steering system will detect this as an FOV-corner event. When this detected corner marks the start of the FOV, it is called an FOV-start event. The CCU uses these events to time the laser pulse transmission of the Transmission Stage. The red areas in the figure indicate dead zones. These are margins within which the laser might hit a mirror corner, which would make the measurement invalid. The CCU will not send.

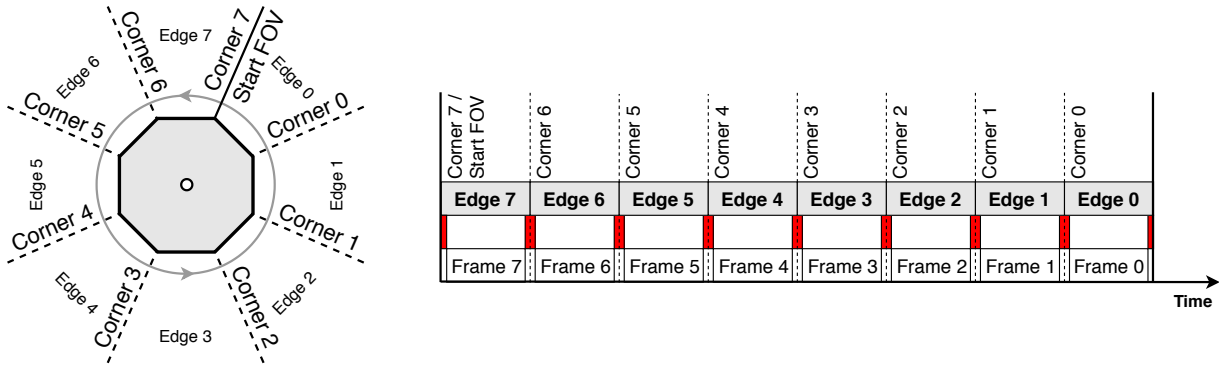


Figure 2.8: Illustration of the correspondence between polygon mirror rotation and pulse timing.

## 2.9.2. Interface specification

The high-level functional overview of each subsystem (see figure 2.6) can be derived from the discussion in section 2.9. Table 2.7 shows the data flow between subsystems. This table assumes the use of the AS6501 TDC IC.

Table 2.7: Data flow between subsystems from figure 2.6.

From:	To:	Transm. Stage	Reception Stage	Beam Steering
CCU	CCU None	<ul style="list-style-type: none"> <li>Pulse frames</li> <li>Reference signals for the laser driver</li> </ul>	<ul style="list-style-type: none"> <li>Control signals for the threshold computer</li> <li>Oscillator to aid in generation of bias signal for the Avalanche photodiode (APD)</li> <li>Configuration and reference signals for the TDC</li> <li>Pulse frame triggers</li> </ul>	<ul style="list-style-type: none"> <li>Motor start and stop signals</li> </ul>
Transm. Stage	<ul style="list-style-type: none"> <li>Serial LVDS TDC timestamp data (2 channels)</li> </ul>	None	None	None
Beam Steering	<ul style="list-style-type: none"> <li>Indication if motor rotates in steady-state</li> <li>FOV-start and FOV-corner event detections</li> </ul>	None	None	None

# 3

## The receiver stage

The receiver stage captures the backscattered light pulse and generates a pulse when an object is detected. This is then converted to a TDC reading of the event. This is accomplished in three stages:

- Optoelectrical transduction & amplification
- Pulse detection
- Time to digital conversion

We will first motivate this division (section 3.1) and then highlight interesting design details of each of these stages (sections 3.2.1, 3.3, 3.3.1 and 3.3.2). From there, we discuss future work in section 3.3.3.

### 3.1. Systems engineering

#### 3.1.1. Function

The goal of the receiver stage is to detect obstacles from the backscattered light. To this end, first the impulse response must be measured, which is modelled by equation 2.4, reproduced here for reference.

$$p(x) = \eta \cdot \exp\left(\int_0^{x/2} \ln(T(\tau)) d\tau\right)^2 \cdot (1 - T(x/2)) \cdot \beta(x/2) \cdot \frac{A_0}{(x/2)^2} \quad (2.4)$$

In which  $p(x)$  is the reflected optical power received from a certain distance  $x$ ,  $\eta$  is the efficiency of the optical path,  $T(x)$  is the transmissivity,  $\beta(x)$  is the reflectivity and  $A_0$  is the effective receiver area, all as defined in section 2.8.

We assume obstacles are characterised by  $T \rightarrow 0$ . Then detecting obstacles is equivalent to finding  $x$  where  $T(x)$  is low. To this end, the transmissivity should be estimated from the measured backscatter impulse response  $p(x)$ . However, there is another free function in equation 2.4, the reflectivity  $\beta(x)$ . However, as motivated in section 2.8, this can be considered everywhere constant. Since the system determines when a pulse is emitted and  $x = \frac{u_p}{2} \cdot t$  is a function of the time  $t$ ,  $x$  is also known. Then finding low transmissivity regions is equivalent to solving equation 3.1 for  $T(x)$  with all other variables being known.

$$p(u_p \cdot t/2) = \eta \cdot \exp\left(\int_0^{u_p \cdot t} \ln(T(\tau)) d\tau\right)^2 \cdot (1 - T(u_p \cdot t)) \cdot \beta \cdot \frac{A_0}{(u_p \cdot t)^2} \quad (3.1)$$

We will rescale the functions in equation 3.1 in terms of time from hereon for notational convenience. This yields equation 3.2.

$$p(t) = \eta \cdot \exp\left(\int_0^t \ln(T(\tau)) d\tau\right)^2 \cdot (1 - T(u_p \cdot t)) \cdot \beta \cdot \frac{A_0}{(t)^2} \quad (3.2)$$

This calculation has to be implemented in analog electronics, since the adopted TDC based architecture only digitises timing of events, not signal values. This is essentially an analog computer design problem.

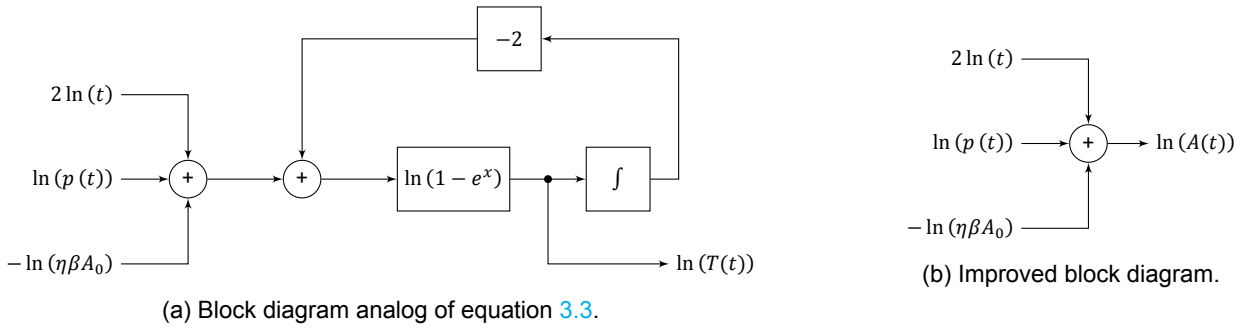


Figure 3.1: Threshold computer block diagrams.

### 3.1.2. Towards a concept design

The most straightforward way to implement such a threshold computer is by interpreting it as an implicit nonlinear state-space model. Since  $\ln(T)$  is in the integral, it is a natural choice of state variable. Rewriting in logarithmic space to avoid tricky-to-implement multiplications and scaling signals to the time domain, this yields equation 3.3.

$$\ln(T(t)) = \ln\left(1 - \exp\left(\ln(p(t)) + 2 \cdot \ln(t) - \ln(\eta \cdot \beta \cdot A_0) - 2 \cdot \int_0^t \ln(T(\tau)) d\tau\right)\right) \quad (3.3)$$

This has a direct block diagram analog, as given in Figure 3.1a.

However, the implementation in figure 3.1a is not feasible, due to two problems. Firstly, it requires a logarithmic amplifier in the signal path. Though these are technically feasible [21] even at the 5 GHz required by RX-PER2b, they are only sold with integrated low pass filters with cutoffs lower than the minimum 500 MHz required by RX-PER2a. This is because they are developed for radio envelope detection.

Secondly, it requires an analog implementation of the function  $f(x) = \ln(1 - e^x)$ , which is hard, but possible using the same segmented nonlinear implementation techniques used in high-bandwidth logarithmic amplifiers. This is however not feasible given the allotted time per PRO1.

The second problem can be solved by observing that sediment tends to settle thanks to the stable environment in the deep sea. This can also be seen in video streams of Remotely Operated Vehicle (ROV) dives [50]. Floating particulates only form in reaction to the thrusters. Given the intended deployment of the LiDAR system on smaller platforms, this is likely not a concern. Then the environment can be expected to be relatively clear. This means that  $\int_0^t \ln(T(\tau)) d\tau$  is small, such that its influence is insignificant. This means that the integral modelling the bulk absorption of the medium can be removed. This still leaves the function of  $f(x) = \ln(1 - e^x)$  to calculate  $\ln(T(t))$  from the result of the summation. However, observing that taking  $f(x) = \ln(1 - e^x) = \ln(T(t))$  gives  $x = \ln(1 - T(t)) = \ln(A(t))$ , which is simply the logarithm of the absorbance of the channel at  $t$ . This is also usable as for simple threshold detection, though the polarity of the comparator needs to be switched. This yields the simplified diagram in figure 3.1b.

This leaves the problem of the high-speed baseband logarithmic amplifier. This can be solved the position of the signal elements. We start by writing out the detection condition of the improved block diagram in equation 3.4.

$$\ln(A(t)) = \ln(p(t)) + 2 \cdot \ln(t) - \ln(\eta \cdot \beta \cdot A_0) > C \quad (3.4)$$

In which  $C$  is the threshold constant. This can be rewritten as in equation 3.5.

$$p(t) > \frac{e^C \cdot \eta \cdot \beta \cdot A_0}{t^2} = p_{max}(t)/\alpha \quad (3.5)$$

This is a simple comparison of the incoming signal with a threshold. This motivates a division of the target detection in a threshold generation circuit and a comparator. Like in section 2.8, we can describe the threshold relative to the maximum returned power using a factor  $\alpha$ . The higher alpha, the higher the resilience to attenuation in the signal path, but also the higher the susceptibility to backscatter and thus the higher the minimum range, as described in section 2.8.

A channel estimator is needed to provide input to the target detector. Since the training signal is a bandwidth-limited delta pulse, this is trivial and implicit in the bandwidth limit of the target detector circuitry.

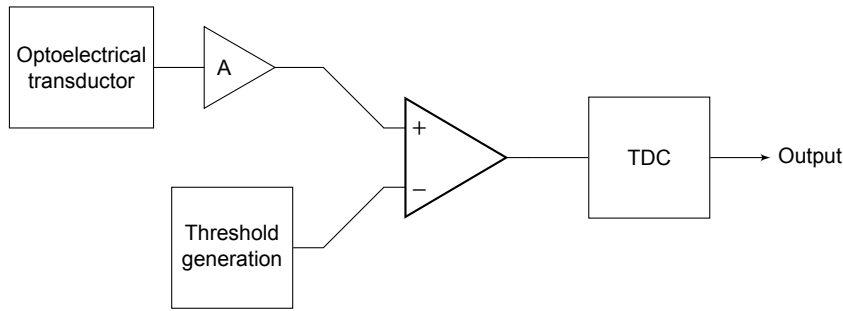


Figure 3.2: Receiver stage concept design

A TDC is required to convert target detection event to a timestamp. An optoelectrical transducer is required to convert the incoming optical signal to an electrical signal. Finally, amplification may be required to provide sufficient input power for the comparator.

The concept design is shown in Figure 3.2.

### 3.1.3. Requirements

In order to fully dimension the receiver stage, we need to derive some more detailed requirements from the system-level requirements. The threshold value needs to be fixed, along with a maximum probability of false detection and the input dynamic range. These are given in Table 3.1.

Table 3.1: Subsystem requirements

ID	Requirement	Verification	Justification
		Test Demonstration Analysis Inspection	
RX-PER3	The threshold of the RX stage shall be $\frac{1}{\alpha} = \frac{1}{6} \pm 50\%$ of the maximum returned power.	•	Maximise sensitivity whilst guaranteeing no susceptibility to backscatter for sizes larger than the minimum range per PER2-a.
RX-PER4	The probability of false reception shall be less than 0.01%	•	Limit spurious readings.
RX-PER5	The receiver stage shall have a dynamic range of over 70 dB	•	Dynamic range required to fit the minimum threshold specified by RX-PER1 and the maximum threshold computed from RX-PER3 whilst guaranteeing ample margin for fulfilment of requirement RX-PER4.

## 3.2. Implementation

We will now briefly discuss the implementation of each of the components.

### 3.2.1. Optoelectrical transduction design

There are 4 types of photodetectors commonly used in LiDAR systems:

- PIN photodiodes, where incoming photons create electron hole pairs, thus generating currents.
- APDs are highly reverse-biased photodiodes, employing the avalanche effect to provide a gain of the generated current.
- Single-Photon Avalanche Diodes (SPADs) has a reverse bias voltage that is well above the breakdown voltage, such that even a single photon can trigger breakdown, giving extremely high amplification. However, a 'quenching circuit' is required to halt the breakdown [13]. Photomultiplier Tubes (PMTs) belong to the class of vacuum tubes. They operate using the photoelectric effect. [22] However, they cannot handle the 100 bar pressure required by ENV1-a due to their internal vacuum chamber.

Though an SPAD solution would be best for the sensitivity required to fulfil [RX-PER1](#), the photon counting is prohibitively difficult for higher intensities. Hence, in order to be able to fulfil [RX-PER5](#) we selected an APD. We selected the C30737LH-500-80A for the highest spectral response at 532 nm of the APDs available at Digikey. A transimpedance amplifier was required to convert the generated currents to voltages for further processing. We used the TIDA-01350 high speed linear transimpedance amplifier reference design [60] for prototyping. At a bandwidth of 3 GHz, it meets [RX-PER2a](#). It also aids in matching the noise of the APD to the comparator.

### 3.3. TDC selection

There are several ICs implementing time to digital conversion, aptly named Time to Digital Converters (TDCs). These are listed in table 3.2. We selected the cheapest TDC which is both in stock and has a sufficiently high maximum sample rate to fulfil [PER11-b](#), [PER6-b](#), [PER7-b](#) and [PER8-b](#). This is the AMS AS6501. We followed the recommended application guidelines from its datasheet.

Table 3.2: List of TDC ICs. Maximum sample rates were estimated from data rate and assuming a transfer of 48 bit per sample, when not given on datasheet. World stock estimated from Findchips on 19/04/2019. Market average prices estimated from Findchips on 19/04/2019.

Part number	Manufacturer	Maximum sample rate	Stock estimate (thousands)	Price
TDC7200	Texas Instruments	< 0.4 MHz	250	\$1.85
TDC7201	Texas Instruments	< 0.5 MHz	7	\$3.15
AS6500	AMS	1.5 MHz	0	\$25
AS6501	AMS	70 MHz	0.5	\$38.14
TDC-GPX	AMS	200 MHz	0.5	\$170
TDC-GPX2	AMS	70 MHz	1.8	\$55
MAX35101	Maxim Integrated	< 0.4 MHz	2	\$6.37

#### 3.3.1. Comparator design

Sadly, high speed comparators all have unacceptably high offset voltages. A solution is to bias the comparator to remove this offset, using negative feedback at low frequencies. However, the compared signals have DC components, which prevents this solution from being usable. Luckily, the signal path does not need to be used continuously, so that the bias can be calibrated whilst it is not in use. Figure 3.3 shows the comparator with negative feedback biasing calibration mode. Attenuation was added to ensure sufficient gain margin for stable calibration.

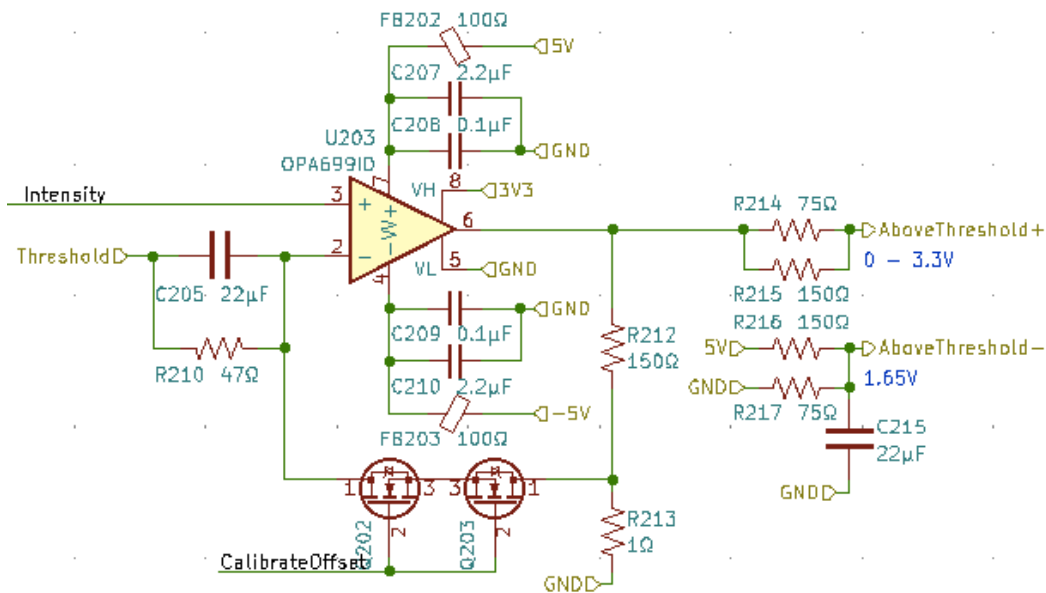


Figure 3.3: Comparator circuit

### 3.3.2. Threshold generation

Generating a  $1/t^2$  pulse is a tricky problem. We considered 5 approaches:

- Direct digital synthesis.
- Using analog power computer circuits on a ramp signal.
- Using a nonlinear amplifier on a ramp signal.
- Using a piecewise linear approximation from a constant current sources in a capacitors.
- Using a piecewise linear approximation in logarithmic space using RC circuits with variable resistance.

The problem with direct digital synthesis is the complexity along with the high resolution required to meet the needed dynamic range as per [RX-PER5](#). Analog power computer circuits generally do not have sufficient bandwidth to compute a sufficiently fast  $1/t^2$  falloff. The design of a nonlinear amplifier would take too much time. Inaccuracies in the timing of a piecewise linear approximation could introduce offsets which would shift the required threshold of [RX-PER1](#) unacceptably. The solution is to do the piecewise approximation in logarithmic space. When there is an inaccuracy in timing, it will not translate to a constant offset but to a difference in the multiplication factor. This ensures the relative inaccuracy remains bounded.

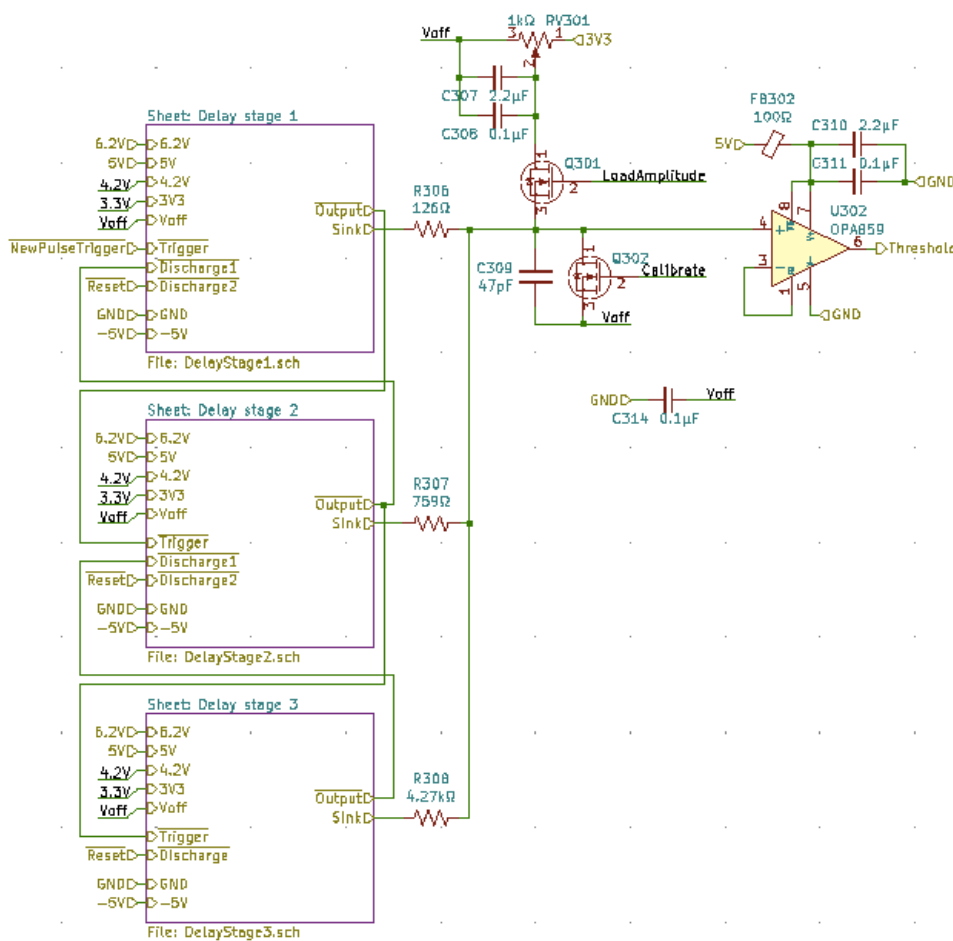


Figure 3.4: The threshold generation circuit.

Such an approximation can be made using a first order circuit and varying the component values. We used an RC circuit, varying the resistance. The resistance was varied by sinking current through one of three different resistors and cycling through these, as illustrated in figure 3.4. The timing requirements are more precise than achievable with the digital system, so an analog timing system was implemented. It is based on 3 delay stages consecutively triggering each other and deactivating the previous stages. The output of the stages had to be buffered to support the high current peaks drawn in the RC circuit. For this, we used a high speed MOSFET driver IC. A single delay stage is shown in figure 3.5.

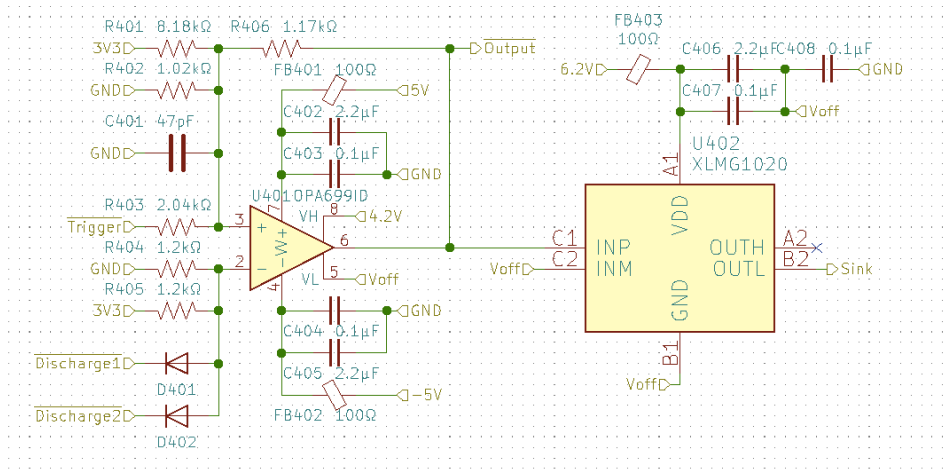


Figure 3.5: A single delay stage.

### 3.3.3. Future work

The performance of the receiver stage remains to be validated. Slew rate limitations in the opamps could introduce walk errors in the timing, which should be investigated. The proposed design for generating high speed  $1/t^2$  pulses should also be checked.

The component values can be expected to drift under pressure, such that piecewise approximation of the threshold in logarithmic space will also drift, which could affect the performance. Ratiometric design techniques should be explored to prevent these effects adversely affecting performance. Nonlinear amplification of ramp generators could be such a technique.

# 4

## Central Control Unit (CCU)

### 4.1. Introduction

The term Central Control Unit (CCU) encompasses all digital logic used for the onboard control, scanning synchronisation and system configuration within the electrical system of the LiDAR. It handles:

- activation of the Transmission Stage, the interpretation of TDC measurements, and the communication of the distance measurement data with an external computer.
- the configuration of itself and the TDC at system boot-up.
- the generation of reference and control signals used in both the transmission and reception stages of the LiDAR system, as well as the motor stage.

The LiDAR subsystem division in figure 2.6 splits the CCU into two parts. The Motor Interface and Motor Controller are designed and implemented by the Beam Steering subgroup. All other modules are designed and implemented by the Reception Stage subgroup in this chapter of this thesis.

This chapter will start by providing the design requirements of the CCU in section 4.2 as derived from previously mentioned criteria and requirements. After that, the high-level design procedure will be elaborated in section 4.3. The VHDL implementation of the design is then verified by means of simulation and then tested on an FPGA, which is explained in section 4.4.

### 4.2. Requirements

The design requirements of the CCU are listed in table 4.1 together with their justification and verification method. They are derived from the CCU tasks specified in the introduction (section 4.1) and the LiDAR requirements from table 2.1.

Table 4.1: Design requirements of the CCU and their justification

ID	Requirement	Verification				Justification
		Test	Demonstration	Analysis	Inspection	
CCU-FUN1-a	All major system parameters should be configurable.					Enables adjustment of data rate, scanning frequency, and FOV. (Req. FUN3)
CCU-FUN1-b	The number of FOV scans per scan routine shall be configurable.					
CCU-FUN2-a	The system shall be able to operate in 2 modes: MODE-0D and MODE-2D.					Enables control over scanning resolution. (Requirement FUN3)
CCU-FUN2-b	In MODE-0D, the system shall perform distance measurements at one coordinate only.					Feature: Enable scanning of a single point for obstacle detection applications
CCU-FUN2-c	In MODE-2D, the system shall perform distance measurements at all coordinates in the FOV.					Feature: Enable scanning of a plane for 3D mapping applications.

*Continued on next page*

Table 4.1 – Continued from previous page

ID	Requirement	Verification			Justification
		Test	Demonstration	Analysis Inspection	
CCU-FUN3	All digital logic within the LiDAR electrical system shall be configured when the system is turned on.	•			Ensures all CCU components work as intended.
CCU-INF1-a	The system shall be able to stream measurement data via a serial data protocol.	•			Measurement packages are too large for a parallel data protocol. (Req. INF3-a, CCU-PER1-a, CCU-PER1-b, CCU-PER2 )
CCU-INF1-b	The system shall be designed modularly in such a way that the serial measurement data interface can be swapped with a 100BASE-TX ethernet interface.		•		High data rate serial protocol, estimated to be fast enough for the LiDAR. (Req. INF3-b)
CCU-INF2	The system shall be able to configure the AS6501 TDC, generate reference signals for it, and read its data out.	•			The AS6501 TDC is used in the reception stage of the LiDAR.
CCU-INF3	The system shall be able to start and stop the motor of the polygon mirror and read out its rotational position.	•			Keeps all control central within the CCU.
CCU-INF4	The system shall generate PWM voltage pulses which the transmission stage will convert to laser pulses.	•			Keeps all control central within the CCU.
CCU-INF5	The system shall generate the timing related reference signals for all analogue electronics within the LiDAR system.	•			Keeps all control central within the CCU.
CCU-INF6	The polygon mirror shall rotate with steady-state angular velocity during distance measurements.	•			Coordinates of transmitted pulse are predictable by means of linear interpolation.
CCU-TEC1	The system shall fit on a 10CL025YE144I7G FPGA.	•			Pressure tolerant FPGA with 50MHz/100MHz clock with enough logic elements to fit the worst case estimate of the design resource usage. (Req. ENV1-a, ENV1-b, ENV2-a, ENV2-b, ENV3, ENV4)
CCU-PER1-a	The system shall have minimum azimuthal resolution of 11 bits.	•			$\lceil \log_2(180^\circ/0.1^\circ) \rceil = 11$ (Req. PER6-a, PER6-b, PER7-a, PER7-b)
CCU-PER1-b	The system shall have zenithal resolution of 3 bits.	•			$\lceil \log_2(8\text{mirror edges}) \rceil = 3$ (Req. PER6-a, PER6-b, PER8-a, PER8-b)
CCU-PER2	The system shall have a minimum distance resolution of 16 bits.	•			$\lceil \log_2(40\text{m}/1\text{mm}) \rceil = 16$ (Req. PER1-a, PER1-b, PER2-a, PER2-b, PER3-a, PER3-b, PER5-a, PER5-b)
CCU-COS1	The design has to be implemented and tested within 8 weeks.				Time constraints of the BAP.

### 4.3. CCU Design

In this section, the top-level design of the CCU will be explained step by step first. After proposing a high-level hardware architecture, the remaining sections will elaborate on the design of the major blocks of this architecture, the only exception being the Motor Interface. In the light of the scale of the CCU, this section will not go into the implementation of common hardware modules. The CCU implementation is then verified by means of simulation.

#### 4.3.1. CCU Top-level

From requirement [CCU-FUN3](#) it follows that the CCU and the TDC need to be configured before a scan can start. Also, the reference signals for the TX stage, RX stage and the TDC need to be enabled. To ensure that this is always the case, the configuration and enabling of reference signals can be done during a boot-up routine as soon as the system is powered.

When the user starts an FOV scan, first the motor has to be started. Requirement [CCU-INF6](#) then demands that the motor turns with steady-state angular velocity before a scan routine can be entered by the system. The chosen polygon mirror has 8 edges (see figure [2.8](#)). An FOV corner is detected by the motor interface when a corner of the mirror passes the line-of-sight of the transmitted laser beam. Until the next FOV corner is detected, a frame of multiple laser pulses can be transmitted onto the particular mirror edge. The FOV corner of the first edge of the mirror is called the FOV start. When an FOV start is detected, an FOV scan routine will be entered. During an FOV scan

routine the transmission stage should be instructed to send one pulse train per mirror edge. For each pulse in that frame, the received TDC data should be acquired, and the corresponding distance measurement should be sent to the user.

The scan routine of the LiDAR follows from the above discussion. The diagram in figure 4.1 shows the event sequence during a scan routine. Once the system is powered, it boots, and goes idle. When the user sends a scan trigger, the motor should start, and the scan can begin once the motor rotates in steady-state (SS). The CCU waits for an FOV start event, and sends a pulse frame for all mirror edges per rotation. For every sent pulse, the TDC is read out, the ToF is computed, and the measurement data is sent to the user.

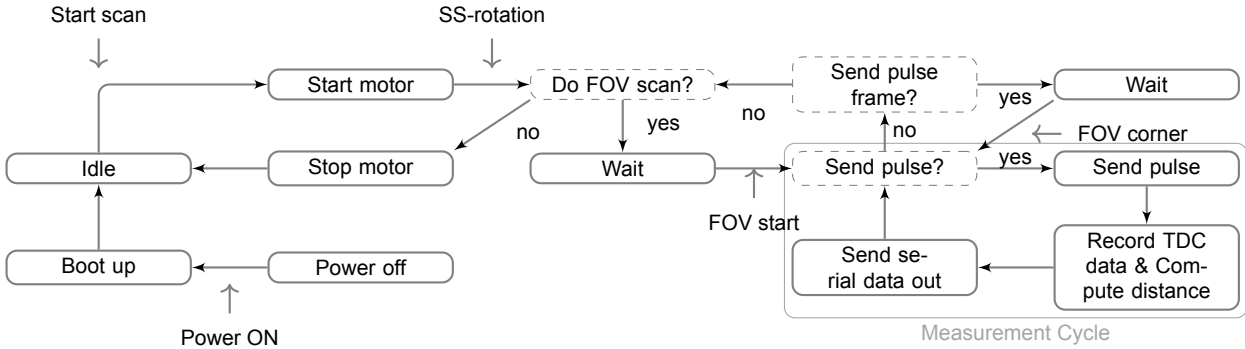


Figure 4.1: Event sequence block diagram of the CCU. An event can be a state of, an action performed by, or a decision made by the CCU. The sequence is based on the configuration of the CCU and external events.

The measurement cycle time  $T_{mc}$  is the time to complete one measurement cycle. It depends on the pulse timeout time  $T_{pulse}$ , the time after which we assume the light pulse will not be detected anymore. The fetching of TDC data, computation of the measured distance, and serial transmission of the measurement data takes processing time  $T_{proc}$ . A measurement cycle can be done in two ways:

- A task starts after the previous has finished. In that case  $T_{mc} = T_{pulse} + T_{proc}$ .
- The TDC sends data to a buffer, which is read out after  $T_{pulse}$ . Meanwhile, the TDC data from the previous pulse is used to compute a distance measurement and to send a serial measurement package. By doing the processing while waiting on  $T_{pulse}$ , as long as  $T_{proc} < T_{pulse}$ , it follows that  $T_{mc} = T_{pulse}$ .

The last case is optimal, because allows a higher measurement frequency, and a longer  $T_{pulse}$  per measurement. This increases the maximum distance that can be detected by the LiDAR system if the CCU were the bottleneck for this. The processing steps in the measurement cycle in figure 4.1 will thus be done in parallel with waiting for  $T_{pulse}$ .

Because of this parallelism, it makes sense to assign a separate hardware module for each step. These modules function as an abstraction of the CCU interfaces with the LiDAR transmission stage, TDC, and Serial User Output (SUO). Since the motor is controlled in parallel with the CCU, the motor functionality can also be abstracted to respond to and generate the motor related signals from figure 4.1. The event sequence of a scan can be done by a simple central FSM that controls the CCU interface abstractions. The system boot-up is unrelated to the scanning logic, and can be implemented as a separate module. The CCU subsystem division following from the above discussion is shown in figure 4.2. The specifications, interface requirements and design of each submodule will be explained in the coming sections.

### 4.3.2. Module: Sequencer

The sequencer module controls the following:

- The starting and stopping of the motor.
- The number of subsequent scans per scan request from the user.
- The number of the pulse frames that is transmitted (see figure 2.8).

Each of these tasks is handled by another block in the proposed implementation, shown in figure 4.3. The scan FSM starts and stops the motor. When the angular velocity of the motor shows steady-state behaviour and an FOV start event occurs, it wakes up two counters. One counter tracks the number of the edge in front of the laser beam, as shown in figure 2.8. At each mirror corner, it starts the pulse generator interface module to send a pulse frame. The second counter tracks the number of scans that are to be done before the system goes idle. It decrements when the 0th frame is transmitted.

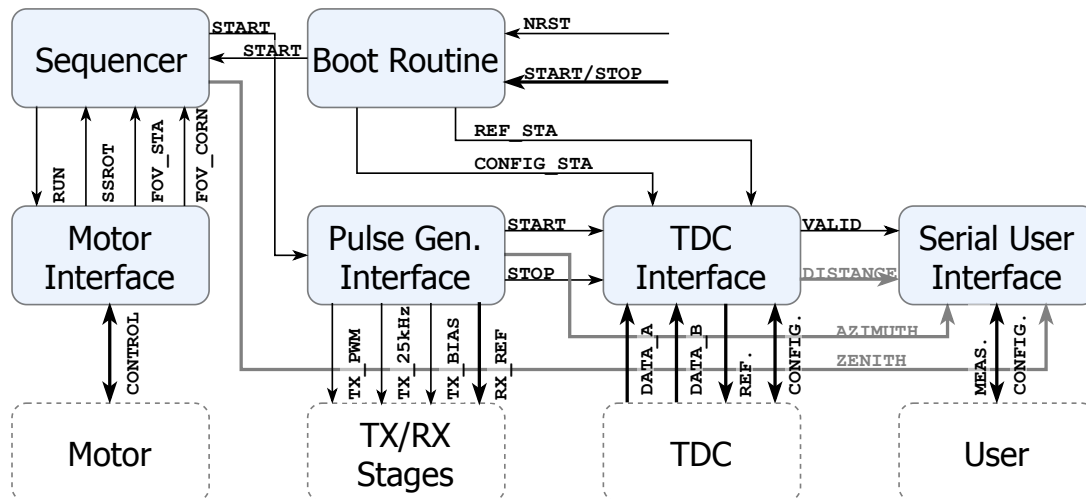


Figure 4.2: Proposed top-level hardware architecture breakdown of the CCU. Blue blocks represent hardware modules implemented on an FPGA. White blocks represent systems external to the FPGA. The names of wires and busses indicates how data flows between blocks. Note that some busses are simplified in the figure.

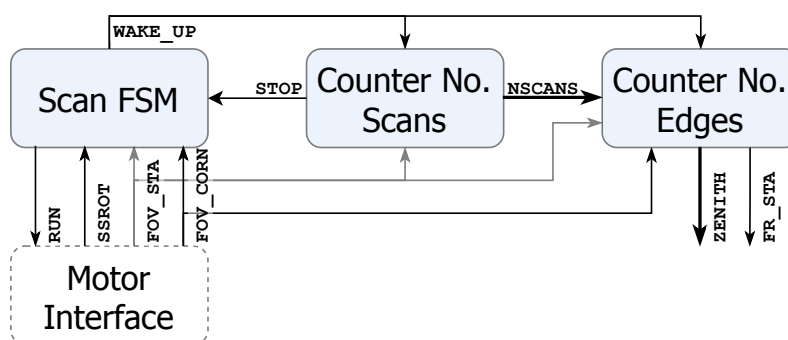


Figure 4.3: Micro-architecture specification of the Sequencer. The implementation details of basic hardware blocks are omitted.

### 4.3.3. Module: Pulse Generator Interface

The main task of the pulse generator interface is to generate a pulse frame. It also generates a 25kHz square wave, a 3.3V DC reference for the APD bias in the transmission stage, and the control signals of the reception stage. In the proposed implementation shown in figure 4.4, the pulse frame is generated by two counters after being triggered by the sequencer. The value of the pulse cycle counter is used to generate a PWM wave with configurable duty cycle and period as well as the reception stage control signals. When the pulse cycle counter finishes, it restarts until the pulse frame ends, and it decrements the pulse train counter. This counter keeps track of the number of pulses that are sent in a frame. Its count values are used to suppress laser pulses from being transmitted if they lie outside the frame boundaries. These boundaries, indicated by the red bars in figure 2.8, ensure the laser does not hit a corner of the mirror, since that would split the beam and make the measurement invalid. If all bits of `FRAME_MR_MAX` are 1, the PWM wave will be indefinite, and continuous. This option is convenient for debugging. Lastly, the `MOD0D_MR` indicates the value of the pulse train counter only for which a pulse will be transmitted in single point scanning mode.

### 4.3.4. Module: TDC Interface

The TDC interface has the following tasks:

- To configure the AS6501 TDC.
- To generate reference signals for the AS6501 TDC so that it can perform time measurements.
- To deserialise the serial LVDS data output of the AS6501 TDC.
- To use the deserialised data to compute a measurement distance estimate.

The proposed implementation is shown in figure 4.5. During system boot-up, the TDC configuration controller is triggered. It sends a stream of bytes from a ROM with configuration data via SPI to the AS6501. During boot-up, the reference signal generator is also triggered, to generate the serial clock, and the measurement reference clock of the TDC.

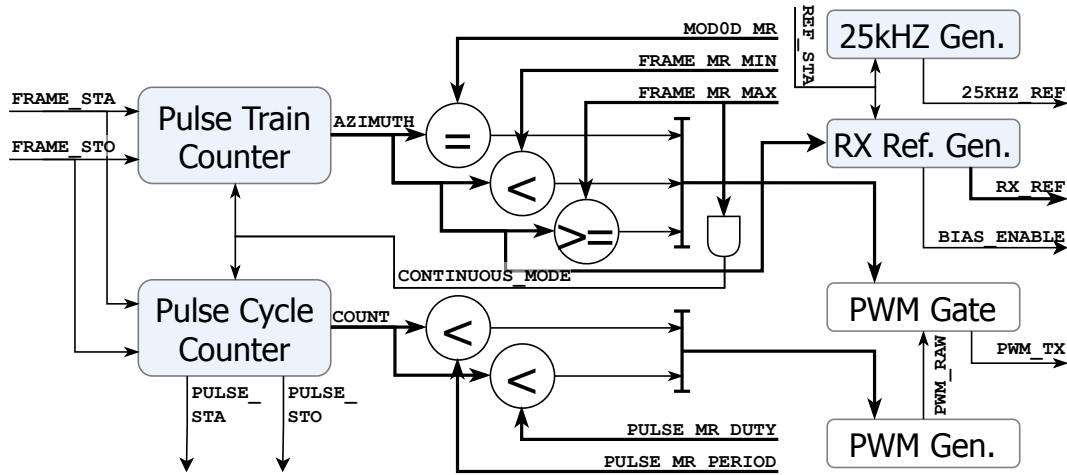


Figure 4.4: Micro-architecture specification of the Pulse Generator Interface. Blue blocks represent sequential logic, whereas white blocks are purely combinational. The implementation details of basic hardware blocks are omitted.

Two LVDS deserialisation modules deserialise the serial LVDS data output from the TDC. Using the pulse-start and pulse-stop trigger from the Pulse Generator Interface, it passes the first TDC measurement values per transmitted pulse to an arithmetic pipeline, which computes a measurement distance estimate. The distance estimate computation is pipelined for three reasons:

- The effective computation time is decreased, which allows reuse of the pipeline when the measurement frequency is increased in the future.
- The worst negative slack timing constraints of the FPGA will likely not be violated because the critical path of the pipeline can be made shorter than that of a purely combinational implementation.
- It allows for easy expansion of the pipeline in case real-time distance measurement calibration needs to be added.

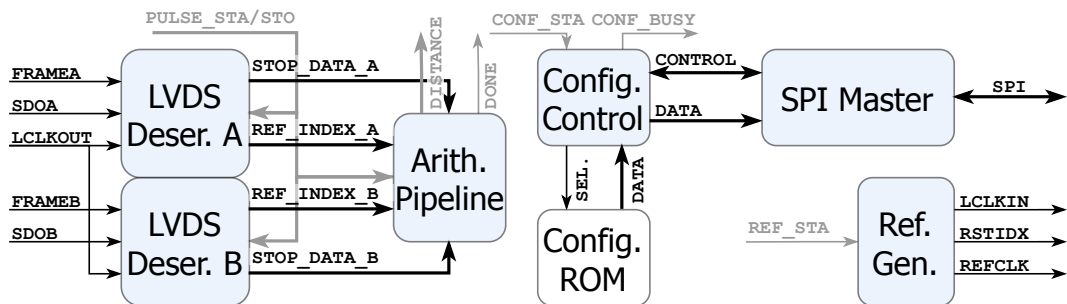


Figure 4.5: Micro-architecture specification of the TDC Interface. Blue blocks represent sequential logic, whereas white blocks are purely combinational. The implementation details of basic hardware blocks are omitted.

### 4.3.5. Module: Serial User Interface

The Serial User Interface is used to:

- Stream measurement data from the LiDAR to the user. A measurement data package is comprised of the polar coordinates of a measurement point. The azimuthal coordinate is represented by 12 bits, the zenithal coordinate by 3 bits, and the radius or distance by 16 bits (see requirements [CCU-PER1-a](#), [CCU-PER1-b](#), [CCU-PER2](#) ). Hence a package contains 31 bits of information.
- Allow the user to configure the LiDAR.

Table 4.2 shows a list of the serial data protocols that we considered together with their advantages and drawbacks. The 10CL025YE144I7G FPGA has enough pins left for any of the listed protocols when taking into account all pins used by the transmission and reception stage, and the motor stage. Due to the limited time to implement the design, a low-complexity protocol is favourable. An SPI master has to be implemented for the configuration logic of the TDC. In addition, SPI protocol is relatively simple. A package of 31 bits is sent as four separate bytes, each taking a minimum

of 10 clock cycles. The maximum measurement rate that the SPI protocol allows assuming a serial clock frequency of 10MHz, common rate of microcontroller SPI peripherals, is  $10\text{MHz}/10/4 = 250\text{kHz}$ .

Table 4.2: List of common serial data protocols and how they compare. ++ means high max. data rate or low complexity, and – means low max. data rate or high complexity.

Protocol	Max. data rate	Complexity	Duplex	Pins used	Comments
CAN	-	-	Half	2	Not as commonly supported by computers or microcontrollers as other protocols.
Ethernet	++	-	Half	4 or 8	Too complex to implement. IP cores required.
I2C	-	+	Half	3 + N	
SPI	-	++	Full	3 + N	SPI master must be implemented for configuration of the AS6501 TDC.
USB 2.0	+	+	Half	2	

## 4.4. Testing and Validation

The VHDL implementation of the CCU toplevel design shown in figure 4.2 is functionally verified using a testbench. This testbench has the following features:

- It checks if all output ports of the design are low during boot-up.
- It emulates the behaviour of the AS6501 TDC.
  - It delays the incoming serial clock (`LCLKIN`).
  - It checks if the TDC configuration SPI stream is generated correctly.
  - It generates random ToF values, composes data frames from them, and serialises them.
- It emulates the behaviour of the Motor Interface.
  - It responds to the motor-start and motor-stop flags.
  - It generates the FOV-start and FOV-corner indicators.
  - It simulates the motor rotating with steady-state angular velocity.
- It checks if the Serial User Interface data corresponds with the distance measurement that should be computed from the randomly generated ToF value from the emulated TDC.

Most requirements from table 4.1 marked as verified using a test are automatically checked during simulation. Only requirements `CCU-FUN2-a`, `CCU-FUN2-b`, and `CCU-FUN2-c` are not checked by the testbench. The testbench is self-checking. Hence, it stops automatically if any check fails. It also provides information about successful tests in the console log of the simulator. The simulation results console log can be found below. The log indicates that all tests are done successfully. The absence of other messages means that all other tests did not fail.

```
# ** Note: TEST_SPICONF: TDC has been configured correctly!
# Time: 112360 ns Iteration: 3 Instance: /slidar_toplevel_tb
# ** Note: TEST_SILCONF: Pulse Generator If., TDC If.,TDC, and Motor If.
  were silent during BOOTUP!
# Time: 112370 ns Iteration: 1 Instance: /slidar_toplevel_tb
```

## 4.5. Future Work

With a design working in simulation only, a number of steps need to be taken before this CCU design is fully verified:

- The design needs to be extensively tested on an FPGA, preferably as integrated with all components within the LiDAR system. The functionality of MODE-2D and MODE-0D (requirement `CCU-FUN2-a`) would take too long to simulate, hence they should be tested on an FPGA.
- An FPGA test with the whole LiDAR system would also enable the verification of the LiDAR itself.

To make the LiDAR more user friendly, the User Interface needs to be revised.

- The SPI master in the User Interface module needs to be replaced by an Ethernet interface to allow for faster measurement data transfer.
- The major parameters that affect the resolution, scan rate and FOV dimensions can be made configurable by the user. To this end, a CCU configuration memory needs to be implemented.

# 5

## Conclusion

In this report, we put forward detailed design considerations of the receiver stage and Central Control Unit (CCU) of a deep sea LiDAR system. We paid particular attention to the system design leading to their configuration, selecting a fairly simple architecture because of time constraints. We discussed and quantified the problem of volumetric backscatter. A potential solution was found in constant transmissivity thresholding, which we showed to reduce to intensity thresholding with a  $1/t^2$  pulse under reasonable assumptions. We highlighted an analog implementation, chosen to minimise system complexity. We also documented a reference implementation for a LiDAR controller, adaptable to a multitude of system architectures. Particular attention was paid to the modularity. The reference implementation also contains the first reference implementation of a VHDL interface to the AS6501 TDC.

A lot of work still remains to be done. We were not able to test compliance with or even meet all our requirements, but the developments in this report can be regarded as a first step towards inexpensive deep sea LiDAR. We hope this will aid the advent of inexpensive autonomous deep sea exploration.

Our aim is to continue developing this technology in the context of underwater localisation and navigation with the end goal of a deep sea SLAM demonstration in the natural environment. To this end, particular attention should be paid to increase the pressure stability of the threshold computer and general subsystem validation. It may also be worth exploring the applicability of recent developments in LiDAR system architectures to deep sea LiDAR, which we were unable to do due to time constraints.

All in all, the developments presented in this report do not definitively demonstrate the feasibility of deep sea LiDAR systems, but represent a good overview of the challenges and possibilities of deep sea LiDAR.

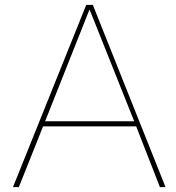
# Bibliography

- [1] 2GRobotics. *ULS-500 PRO Dynamic Underwater Laser Scanner*. URL: <https://www.2grobotics.com/products/underwater-laser-scanner-uls-500/>.
- [2] A. Almslmany et al. "Time varying gain amplifier linearity enhancement for wide dynamic range in radar receiver". In: *Proceedings of 2015 IEEE MTT-S International Conference on Numerical Electromagnetic and Multiphysics Modeling and Optimization, NEMO 2015*. IEEE, Aug. 2016, pp. 1–4. ISBN: 9781479968114. DOI: [10.1109/NEMO.2015.7415022](https://doi.org/10.1109/NEMO.2015.7415022). URL: <http://ieeexplore.ieee.org/document/7415022/>.
- [3] Ery Arias-Castro and Yonina C. Eldar. "Noise folding in compressed sensing". In: *IEEE Signal Processing Letters* 18.8 (2011), pp. 478–481. ISSN: 10709908. DOI: [10.1109/LSP.2011.2159837](https://doi.org/10.1109/LSP.2011.2159837).
- [4] Shlomi Arnon. "Underwater optical wireless communication network". In: *Optical Engineering* 49.1 (2010), p. 015001. ISSN: 0091-3286. DOI: [10.1117/1.3280288](https://doi.org/10.1117/1.3280288). URL: <http://opticalengineering.spiedigitallibrary.org/article.aspx?doi=10.1117/1.3280288>.
- [5] W.L. Barber and E.R. Brown. "A true logarithmic amplifier for radar IF applications". In: *IEEE Journal of Solid-State Circuits* 15.3 (June 1980), pp. 291–295. ISSN: 0018-9200. DOI: [10.1109/JSSC.1980.1051386](https://doi.org/10.1109/JSSC.1980.1051386). URL: <http://ieeexplore.ieee.org/document/1051386/>.
- [6] *Blackmore LiDAR*. URL: <https://blackmoreinc.com/afdl> (visited on 06/16/2019).
- [7] V. Brandou et al. "3D Reconstruction of Natural Underwater Scenes Using the Stereovision System IRIS". In: *OCEANS 2007 - Europe*. IEEE, June 2007, pp. 1–6. ISBN: 978-1-4244-0634-0. DOI: [10.1109/oceanse.2007.4302315](https://doi.org/10.1109/oceanse.2007.4302315). URL: <http://ieeexplore.ieee.org/document/4302315/>.
- [8] J.D.A. van den Broek. "Design and implementation of an Analog-to-Time-to-Digital converter". PhD thesis. UT Twente, 2012. URL: <http://essay.utwente.nl/69501/1/MSc.%20report%20Broek%20van%20den,%20J.D.A.pdf>.
- [9] J. H.R. Burns and D. Delparte. "Comparison of commercial structure-from-motion photogrammetry software used for underwater three-dimensional modeling of coral reef environments". In: *International Archives of the Photogrammetry, Remote Sensing and Spatial Information Sciences - ISPRS Archives*. Vol. 42. 2W3. Feb. 2017, pp. 127–131. DOI: [10.5194/isprs-archives-XLII-2-W3-127-2017](https://doi.org/10.5194/isprs-archives-XLII-2-W3-127-2017). URL: <https://www.int-arch-photogramm-remote-sens-spatial-inf-sci.net/XLII-2-W3/127/2017/>.
- [10] F. M. Caimi and F. R. Dalgleish. "Performance considerations for continuous-wave and pulsed laser line scan (LLS) imaging systems". In: *Journal of the European Optical Society* 5 (Apr. 2010), 10020s. ISSN: 19902573. DOI: [10.2971/jeos.2010.10020s](https://doi.org/10.2971/jeos.2010.10020s). URL: [https://www.jeos.org/index.php/jeos%7B%5C\\_%7Drp/article/view/10020s](https://www.jeos.org/index.php/jeos%7B%5C_%7Drp/article/view/10020s).
- [11] Jonathan L. Carrivick and Mark W. Smith. "Fluvial and aquatic applications of Structure from Motion photogrammetry and unmanned aerial vehicle/drone technology". In: *Wiley Interdisciplinary Reviews: Water* 6.1 (Jan. 2019), e1328. ISSN: 2049-1948. DOI: [10.1002/wat2.1328](https://doi.org/10.1002/wat2.1328). URL: <https://onlinelibrary.wiley.com/doi/abs/10.1002/wat2.1328>.
- [12] *Coda Octopus, sound underwater intelligence*. URL: <https://www.codaoctopus.com/>.
- [13] Sergio Cova et al. "Avalanche photodiodes and quenching circuits for single-photon detection". In: *Appl. Opt.* 35 (1996), pp. 1956–1976.
- [14] DeepSea Power & Light. *Subsea Cameras*. URL: <http://www.deepsea.com/products/cameras/> (visited on 07/12/2019).
- [15] 3D at Depth. *SL3 Subsea LiDAR Laser*. URL: <https://www.3datdepth.com/product/subsea-lidar-sl3>.
- [16] Edgetech. *EdgeTech Sonar*. URL: <https://www.edgetech.com/products/side-scan-sonar/>.
- [17] Andrew Filisetti et al. "Developments and applications of underwater LiDAR systems in support of marine science". In: *OCEANS 2018 MTS/IEEE Charleston, OCEAN 2018* January (2019), pp. 1–10. DOI: [10.1109/OCEANS.2018.8604547](https://doi.org/10.1109/OCEANS.2018.8604547).
- [18] Miles Hansard et al. *Time of Flight Cameras : Principles , Methods , and Applications*. 2012. DOI: [10.1007/978-1-4471-4658-2](https://doi.org/10.1007/978-1-4471-4658-2). URL: <https://hal.inria.fr/hal-00725654/PDF/TOF.pdf>.

- [19] Duo-Min He and Gerald G.L. Seet. "Divergent-beam Lidar imaging in turbid water". In: *Optics and Lasers in Engineering* 41.1 (Jan. 2004), pp. 217–231. ISSN: 0143-8166. DOI: [10.1016/S0143-8166\(02\)00138-0](https://doi.org/10.1016/S0143-8166(02)00138-0). URL: <https://www.sciencedirect.com.tudelft.idm.oclc.org/science/article/pii/S0143816602001380>.
- [20] Franco Hidalgo and Thomas Braunl. "Review of underwater SLAM techniques". In: *ICARA 2015 - Proceedings of the 2015 6th International Conference on Automation, Robotics and Applications*. IEEE, Feb. 2015, pp. 306–311. ISBN: 9781479964666. DOI: [10.1109/ICARA.2015.7081165](https://doi.org/10.1109/ICARA.2015.7081165). URL: <http://ieeexplore.ieee.org/document/7081165/>.
- [21] Chris D. Holdenried et al. "A DC-4-GHz true logarithmic amplifier: Theory and implementation". In: *IEEE Journal of Solid-State Circuits* 37.10 (Oct. 2002), pp. 1290–1299. ISSN: 00189200. DOI: [10.1109/JSSC.2002.803059](https://doi.org/10.1109/JSSC.2002.803059). URL: <http://ieeexplore.ieee.org/document/1035943/>.
- [22] Burle industries inc. "Photomultiplier Handbook". In: (1980), pp. 8–80. URL: [https://psec.uchicago.edu/links/Photomultiplier%7B%5C\\_%7DHandbook.pdf](https://psec.uchicago.edu/links/Photomultiplier%7B%5C_%7DHandbook.pdf).
- [23] Achuta Kadambi and Petros T. Boufounos. "Coded aperture compressive 3-D LIDAR". In: *ICASSP, IEEE International Conference on Acoustics, Speech and Signal Processing - Proceedings 2015-Augus* (2015), pp. 1166–1170. ISSN: 15206149. DOI: [10.1109/ICASSP.2015.7178153](https://doi.org/10.1109/ICASSP.2015.7178153).
- [24] LeddarTech. *Leddar Optical Time-Of-Flight Sensing Technology*. 2016.
- [25] B. Timothy Lee. "How 10 leading companies are trying to make powerful, low-cost lida". In: *Ars Technica* (2019). URL: <https://arstechnica.com/cars/2019/02/the-ars-technica-guide-to-the-lidar-industry/>.
- [26] Larry Li. *Time-of-Flight Camera—An Introduction*. 2014.
- [27] Jerry Liao. *Bar code reader with polygon mirror having curved reflection surfaces*. Sept. 2005. URL: <https://patents.google.com/patent/US20070069025>.
- [28] Daniel J. Lum, Samuel H. Knarr, and John C. Howell. "Frequency-modulated continuous-wave LiDAR compressive depth-mapping". In: *Optics Express* 26.12 (June 2018), p. 15420. ISSN: 1094-4087. DOI: [10.1364/OE.26.015420](https://doi.org/10.1364/OE.26.015420). URL: <https://www.osapublishing.org/abstract.cfm?URI=oe-26-12-15420>.
- [29] Neil Manning. *Teledyne CDL*. 2014.
- [30] Marco Reys. *All about the Xiaomi Lidar Scanner and the Sunfounder RasPad*. URL: <https://www.youtube.com/watch?v=4sQCz75BfrM> (visited on 06/18/2019).
- [31] Gerald F. Marshall and Glenn E. Stutz. *Polygonal Scanners: Components, Performance, and Design*. 2011, p. 788. ISBN: 1439808791. URL: <http://books.google.com/books?id=MLWUatLv0s0C%7B%5C%7Dpgis=1>.
- [32] Miquel Massot-Campos and Gabriel Oliver-Codina. "Optical Sensors and Methods for Underwater 3D Reconstruction." In: *Sensors (Basel, Switzerland)* 15.12 (Dec. 2015), pp. 31525–57. ISSN: 1424-8220. DOI: [10.3390/s151229864](https://doi.org/10.3390/s151229864). URL: <http://www.ncbi.nlm.nih.gov/pubmed/26694389%20http://www.pubmedcentral.nih.gov/articlerender.fcgi?artid=PMC4721784>.
- [33] Paul F. McManamon et al. "Comparison of flash lidar detector options". In: *Optical Engineering* 56.3 (2017), p. 031223. ISSN: 0091-3286. DOI: [10.1117/1.oe.56.3.031223](https://doi.org/10.1117/1.oe.56.3.031223).
- [34] L. E. Mertens and F. S. Replogle. "Use of point spread and beam spread functions for analysis of imaging systems in water". In: *Journal of the Optical Society of America* 67.8 (Aug. 1977), p. 1105. ISSN: 0030-3941. DOI: [10.1364/josa.67.001105](https://doi.org/10.1364/josa.67.001105). URL: <https://www.osapublishing.org/abstract.cfm?URI=josa-67-8-1105>.
- [35] Michael Watts. *A review of Optical Phased Array LiDAR*. 2018. URL: <https://www.youtube.com/watch?v=H-ZYe2IONOs> (visited on 06/18/2019).
- [36] P M Moser. *Spectral transmission of light through sea water*. Tech. rep. September. Pacific-Sierra Research Corporation, 1992. URL: <http://www.dtic.mil/docs/citations/AD1012965>.
- [37] Pep Lluís Negre, Francisco Bonin-Font, and Gabriel Oliver. "Cluster-based loop closing detection for underwater slam in feature-poor regions". In: *Proceedings - IEEE International Conference on Robotics and Automation*. Vol. 2016-June. IEEE, May 2016, pp. 2589–2595. ISBN: 9781467380263. DOI: [10.1109/ICRA.2016.7487416](https://doi.org/10.1109/ICRA.2016.7487416). URL: <http://ieeexplore.ieee.org/document/7487416/>.
- [38] Newton. *M310UW Dual Usage Laser Scanner*. URL: [https://www.newtonlabs.com/scan%7B%5C\\_%7Dm300uw%7B%5C\\_%7Dsys%7B%5C\\_%7Dspecs.html](https://www.newtonlabs.com/scan%7B%5C_%7Dm300uw%7B%5C_%7Dsys%7B%5C_%7Dspecs.html).
- [39] Nic Bingham. *Designing pressure-tolerant electronic systems*. 2013. URL: <https://www.uutech.com/ptepaper/> (visited on 07/12/2019).

- [40] Takashi; Ogawa and Gerd; Wanielik. "FUSION 2016 : 19th International Conference on Information Fusion : proceedings : Heidelberg, 5-8 July 2016." In: (2016), p. 2337. URL: <https://ieeexplore-ieee-org.tudelft.idm.oclc.org/document/7528061>.
- [41] "Optical phased array lidar system and method of using same". In: (May 2014). URL: <https://patents.google.com/patent/US20160161600A1/en>.
- [42] Ouster. *Ouster Lidar product listing*. URL: <https://www.ouster.io/> (visited on 06/18/2019).
- [43] Bing Ouyang, Fraser R Dagleish, and Anni K Vuorenkoski. *Feasibility Study of Compressive Sensing Underwater Imaging Lidar*. 2014. URL: <https://apps.dtic.mil/docs/citations/ADA622707>.
- [44] Angus Pacala. *How Multi-Beam Flash LIDAR Works (Ouster blog)*. 2018. URL: <https://www.ouster.io/blog-posts/2018/11/8/how-multi-beam-flash-lidar-works> (visited on 06/18/2019).
- [45] Christopher V. Poulton et al. "Coherent solid-state LIDAR with silicon photonic optical phased arrays". In: *Optics Letters* 42.20 (2017), p. 4091. ISSN: 0146-9592. DOI: 10.1364/ol.42.004091.
- [46] Kraken Robotics. *The Kraken SeaVision: 3D RGB Underwater Laser Scanner*. URL: <https://krakenrobotics.com/products/seavision/>.
- [47] Matija Rossi et al. "Real-Time Underwater StereoFusion". In: *Sensors (Basel, Switzerland)* 18.11 (Nov. 2018), p. 3936. ISSN: 14248220. DOI: 10.3390/s18113936. URL: <http://www.mdpi.com/1424-8220/18/11/3936>.
- [48] S Rutten et al. "On the way to a pressure tolerant LiDAR for deep sea robot navigation". In: 4472659 ().
- [49] Davide Scaramuzza et al. "Past, Present, and Future of Simultaneous Localization and Mapping: Toward the Robust-Perception Age". In: *IEEE Transactions on Robotics* 32.6 (2016), pp. 1309–1332. ISSN: 1552-3098. DOI: 10.1109/tro.2016.2624754.
- [50] Schmidt Ocean Institute. *Dive 10 ROV Live Stream Perth Canyon - YouTube*. URL: <https://www.youtube.com/watch?v=JlgsdUfaSNI> (visited on 06/21/2019).
- [51] David J. Segelstein. "The complex refractive index of water". In: (1981). URL: <https://mospace.umsystem.edu/xmlui/handle/10355/11599>.
- [52] Sexton Corporation. *Sexton camera enclosures*. URL: <http://www.thesextonco.com/shop/camera-enclosures/> (visited on 07/12/2019).
- [53] Yoni Sher et al. "Low Intensity LiDAR using Compressed Sensing and a Photon Number Resolving Detector". In: (Feb. 2018). arXiv: 1802.09354. URL: <http://arxiv.org/abs/1802.09354>.
- [54] *Side scan sonar, Klein Marine inc*. URL: <http://kleinmarinesystems.com/products/side-scan-sonar/>.
- [55] Sidus Solutions LLC. *Cameras*. URL: <http://www.sidus-solutions.com/product-category/cameras/> (visited on 07/12/2019).
- [56] Slamtec. *RPLIDAR S1 product listing*. URL: <https://www.slamtec.com/en/Lidar/S1> (visited on 06/18/2019).
- [57] Slamtec. *RPLIDAR-A1 product listing*. URL: <https://www.slamtec.com/en/Lidar/A1> (visited on 06/18/2019).
- [58] SULIS Subsea Corporation. *Products*. URL: <http://www.sulissubsea.com/products/> (visited on 07/12/2019).
- [59] *Teledyne technologies*. URL: <http://www.teledyne.com/>.
- [60] Texas Instruments Incorporated. "High-Speed , Linear Transimpedance Amplifier Reference". In: December (2017), pp. 1–17. URL: <http://www.ti.com/tool/TIDA-01350>.
- [61] Texas Instruments Incorporated. *LIDAR Pulsed Time of Flight Reference Design*. 2018. URL: <http://www.ti.com/tool/TIDA-00663%7B%5C%7Dtechnicaldocuments>.
- [62] A. R. Thurber et al. "Ecosystem function and services provided by the deep sea". In: *Biogeosciences* 11.14 (July 2014), pp. 3941–3963. ISSN: 17264189. DOI: 10.5194/bg-11-3941-2014. URL: <https://www.biogeosciences.net/11/3941/2014/>.
- [63] Timothy B. Lee. *Why spinning lidar sensors might be around for another decade*. 2018. URL: <https://arstechnica.com/cars/2018/05/why-bulky-spinning-lidar-sensors-might-be-around-for-another-decade/> (visited on 06/18/2019).
- [64] Tritech. *Gemini 720im Multibeam Sonar*. URL: <https://www.tritech.co.uk/product/gemini-720im>.
- [65] Velodyne. *Velodyne Puck product listing*. URL: <https://velodynelidar.com/vlp-16.html> (visited on 06/18/2019).

- [66] Wu Xiaochun et al. *Laser radar based on MEMS micro mirror*. Nov. 2015. URL: <https://patents.google.com/patent/CN205120965U/en?q=lidar+mems>.
- [67] Huikai Xie et al. "Wide-angle structured light with a scanning MEMS mirror in liquid". In: *Optics Express* 24.4 (2016), p. 3479. DOI: [10.1364/oe.24.003479](https://doi.org/10.1364/oe.24.003479).
- [68] Fangpei Zhang. "Broad band direct modulation for chirp AM lidar". In: *Optik* 130 (Feb. 2017), pp. 383–392. ISSN: 00304026. DOI: [10.1016/j.ijleo.2016.10.097](https://doi.org/10.1016/j.ijleo.2016.10.097). URL: <https://www-sciencedirect-com.tudelft.idm.oclc.org/science/article/pii/S0030402616312475>.
- [69] Hao Zhang et al. "Bidirectional reflectance measurements of sediments in the vicinity of Lee Stocking Island, Bahamas". In: *Limnology and Oceanography* 48.1part2 (Jan. 2003), pp. 380–389. ISSN: 00243590. DOI: [10.4319/lo.2003.48.1\\_part\\_2.0380](https://doi.org/10.4319/lo.2003.48.1_part_2.0380). URL: [http://doi.wiley.com/10.4319/lo.2003.48.1%7B%5C\\_%7Dpart%7B%5C\\_%7D2.0380](http://doi.wiley.com/10.4319/lo.2003.48.1%7B%5C_%7Dpart%7B%5C_%7D2.0380).
- [70] Xiaoyang Zhang et al. "MEMS mirrors submerged in liquid for wide-angle scanning". In: *2015 Transducers - 2015 18th International Conference on Solid-State Sensors, Actuators and Microsystems, TRANSDUCERS 2015* (2015), pp. 847–850. DOI: [10.1109/TRANSDUCERS.2015.7181056](https://doi.org/10.1109/TRANSDUCERS.2015.7181056).



## The polygon

In the greenlight assessment, the question was raised if the angle of the shaft can be linearly interpolated.

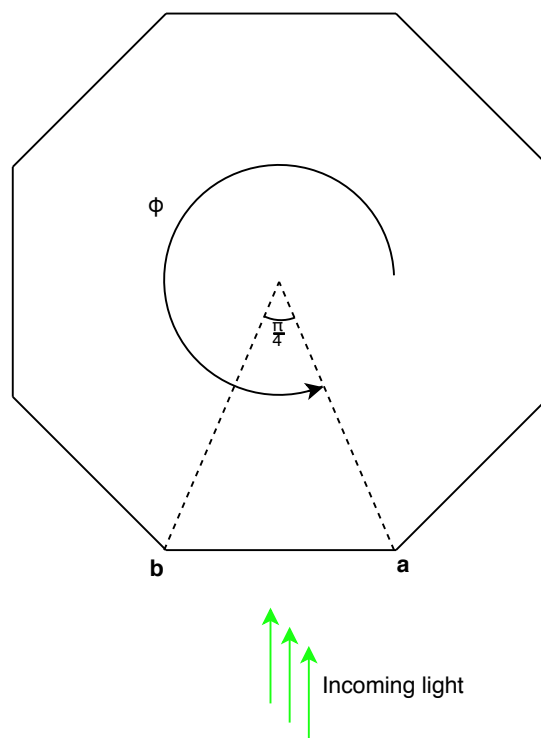


Figure A.1: Simplification of situation to prove angle can be linearly interpolated.

The situation is displayed in figure A.1. The following parameters can be defined.

$$\mathbf{a} = \begin{bmatrix} r \sin(\phi) \\ -r \cos(\phi) \end{bmatrix} \quad \mathbf{b} = \begin{bmatrix} r \sin(\phi - \frac{\pi}{4}) \\ -r \cos(\phi - \frac{\pi}{4}) \end{bmatrix}$$

$$\|\mathbf{a}\| = \|\mathbf{b}\| = r$$

$$ab = \mathbf{b} - \mathbf{a} = \begin{bmatrix} b_x - a_x \\ b_y - a_y \end{bmatrix}$$

Due to symmetry

$$0 \leq \phi \leq \frac{\pi}{4}$$

the normal vector  $\hat{n}$  is  $ab$  shifted by 90 degrees and normalised

$$\hat{n} = \frac{1}{\|\mathbf{b} - \mathbf{a}\|} \begin{bmatrix} a_y - b_y \\ b_x - a_x \end{bmatrix}$$

Because the laser and the centre of the polygon are both in the y-z plane, the incoming light can be modeled as

$$r_i = \begin{bmatrix} 0 \\ 1 \end{bmatrix}$$

$r_o$  is the reflection vector of  $r_i$  over  $\hat{n}$

$$r_o = (r_i - \text{proj}_{\hat{n}}(r_i)) - \text{proj}_{\hat{n}}(r_i) = r_i - 2\hat{n}(\hat{n} \cdot r_i)$$

$$r_o = \begin{bmatrix} 0 \\ 1 \end{bmatrix} + \frac{2a_x - 2b_x}{\|\mathbf{b} - \mathbf{a}\|^2} \begin{bmatrix} a_y - b_y \\ b_x - a_x \end{bmatrix}$$

$$\|\mathbf{b} - \mathbf{a}\|^2 = (b_x - a_x)^2 + (b_y - a_y)^2$$

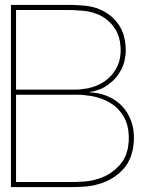
so

$$r_o = \begin{bmatrix} 0 \\ 1 \end{bmatrix} + \frac{2a_x - 2b_x}{(b_x - a_x)^2 + (b_y - a_y)^2} \begin{bmatrix} a_y - b_y \\ b_x - a_x \end{bmatrix}$$

Substituting and simplifying gives

$$r_o = \begin{bmatrix} -\cos(2\phi + \frac{\pi}{4}) \\ -\sin(2\phi + \frac{\pi}{4}) \end{bmatrix} = \begin{bmatrix} \cos(2\phi + \frac{5\pi}{4}) \\ \sin(2\phi + \frac{5\pi}{4}) \end{bmatrix}$$

Clearly, the angle of the reflection is  $2\phi + \frac{5\pi}{4}$  with respect to the x-axis. This means that the angle of the reflected light is linear with  $\phi$  and thus can be linearly interpolated. From this the Field Of View (FOV) can be derived. Because the domain was specified as  $0 \leq \phi \leq \frac{\pi}{4}$ , the horizontal FOV is  $90^\circ$ . It was also known that the vertical angle from one plane to the next differs  $4.5^\circ$ . This means that the vertical FOV is  $36^\circ$ . Unfortunately, this does not meet *shall* requirement [PER6-a](#), but it complies with the minimal [PER6-b](#) requirement.k



## Range Estimation Matlab Code

```
%% define some symbols
syms distance
assume(distance, "positive")

%% system specs
% transmission specs
slope_efficiency.min = 0.6; % W/A
slope_efficiency.max = slope_efficiency.min; % W/A

transmit_current.min = 1; % A
transmit_current.max = 1; % A

% detector specs
effective_area.min = 8e-3 * 17e-3; % m^2
effective_area.max = 8e-3 * 17e-3; % m^2

detector_threshold_current.min = 0.4e-6; % A
detector_threshold_current.max = 0.4e-6; % A

detector_efficiency.min = 8; % A/W
detector_efficiency.max = 8; %0.25; % A/W

% efficiencies
angular_efficiency.min = cos(deg2rad(75 / 4)) * 0.4;
angular_efficiency.max = 1;

hole_efficiency.min = 0.95;
hole_efficiency.max = 0.95;

optical_efficiency.min = 0.9;
optical_efficiency.max = 0.9;

% target specs
albedo.min = 0.1;
albedo.max = 0.2;

% medium specs
water_transmission.min = 0.95; % Np/m
water_transmission.max = 0.95; % Np/m

%% find rx current
efficiency.min = angular_efficiency.min * hole_efficiency.min * ...
                 optical_efficiency.min;
efficiency.max = angular_efficiency.max * hole_efficiency.max * ...
                 optical_efficiency.max;

medium_transmission.min = water_transmission.min^(2*distance);
medium_transmission.max = water_transmission.max^(2*distance);

% assumes lambertian full reflectance
spread.min = effective_area.min / (2 * pi * distance^2);
spread.max = effective_area.max / (2 * pi * distance^2);

transmission.min = efficiency.min * medium_transmission.min * spread.min * albedo.min;
```

```

transmission.max = efficiency.max * medium_transmission.max * spread.max * albedo.max;

tx_power.min = transmit_current.min * slope_efficiency.min;
tx_power.max = transmit_current.max * slope_efficiency.max;

rx_power.min = transmission.min * tx_power.min;
rx_power.max = transmission.max * tx_power.max;

rx_current.min = rx_power.min * detector_efficiency.min;
rx_current.max = rx_power.max * detector_efficiency.max;

%% find distance
expected_distance.min = vpsolve(rx_current.min == detector_threshold_current.max, distance, 0.1);
expected_distance.max = vpsolve(rx_current.max == detector_threshold_current.min, distance, 0.1);

expected_distance.min
expected_distance.max

```